Comparison of the rheology of bubbly liquids prepared by whisking air into a viscous liquid (honey) and a shear-thinning liquid (guar gum solutions)

M.D. Torres[a,b], F. Gadala-Maria[a,c] and D.I. Wilson[a]

[a]Department of Chemical Engineering and Biotechnology, New Museums Site, University of Cambridge, Pembroke St, Cambridge, CB2 3RA, UK.

[b]Department of Chemical Engineering, University of Santiago de Compostela, Lope Gómez de Marzoa St, Santiago de Compostela, E-15782, Spain.

[c]Department of Chemical Engineering, University of South Carolina, Columbia, SC 29208, USA.

Submitted to

J. Food Engineering

March 2013

Revised Manuscript

Comparison of the rheology of bubbly liquids prepared by whisking air into a viscous liquid (honey) and a shear-thinning liquid (guar gum solutions)

M.D. Torres · F. Gadala-Maria · D.I. Wilson

Abstract

Many bubbly liquids found in food applications feature non-Newtonian liquid phases whereas most investigations of bubbly liquid rheology bulk have employed Newtonian liquids as the continuous phase. The influence of the nature of the continuous phase on bubbly liquid rheology was investigated using bubbly liquids prepared in the same planetary mixer using a viscous liquid, honey (almost constant shear viscosity with a small elastic contribution) and a shear-thinning liquid (1 wt% aqueous solution of guar gum). The viscosity of the honey was similar to the low-shear-rate limit viscosity of the guar gum solution. Although similar bubble volume fractions (up to 25%) were entrained in each liquid under identical mixing conditions, the bubble diameters in the shear-thinning liquid were about two to three times larger than those in the honey. Introduction of a surfactant into the shear-thinning liquid increased the volume fraction of bubbles to approx. 40% and further increased the size of the bubbles. The presence of the bubbles in the honey caused it to become shear-thinning, to exhibit noticeable elastic effects and exert significant normal stress differences. The honey-based bubbly liquids exhibited many of the features in the simulations of Loewenberg and Hinch (1996) and fitted the model of Llewellin *et al*. (2002) well. In the guar gum solution, these characteristics, already present, were accentuated strongly by the presence of the bubbles. Subjecting both types of bubbly liquids to high shear rates caused the volume fraction of bubbles to decrease and made the bubbly liquids less shear-thinning. Noticeable thixotropy was observed. Shear-thinning, associated with bubble deformation, was observed at lower values of the relative shear stress in the shear-thinning liquid.

Keywords Bubbly liquid · Elasticity · Guar gum · Honey · Normal forces · Viscosity

M.D. Torres
Department of Chemical Engineering, University of Santiago de Compostela,
Lope Gómez de Marzoa St, Santiago de Compostela, E-15782, Spain.

F. Gadala-Maria
Department of Chemical Engineering, University of South Carolina, Columbia, SC 29208, USA.

D.I. Wilson (✉)
Department of Chemical Engineering and Biotechnology, New Museums Site, University of Cambridge,
Pembroke St, Cambridge, CB2 3RA, UK,
e-mail address: diw11@cam.ac.uk

Nomenclature

Roman

a	fitting parameter, Szyszkowski equation, N m^{-1}
a'	dimensionless parameter, -
a_1, a_2	parameters, equation [17], -
b	fitting parameter of Szyszkowski equation, mol dm^{-3}
b'	dimensionless parameter, -
C	concentration, mol dm^{-3}
Ca	capillary number, -
d_{max}	largest measured bubble diameter, m
d_{min}	smallest measured bubble diameter, m
F_{normal}	normal force generated by the flow between plates, N
k	time constant, s^{1-n}
K	dimensionless parameter, -
G'	storage modulus, Pa s
G''	loss modulus, Pa s
n	flow index, -
n_b	number of bubbles, -
N_1	first normal stress difference, Pa
N_2	second normal stress difference, Pa
N_c	number of classes of bubbles, -
r	radius of the undeformed bubble, m
R_{pp}	radius of parallel plate geometry, m
R^2	square of the correlation coefficient, -
T	torque, N m
w	class interval width, m
Wi	Weissenberg number, -
x	variable, equation [17], -

Greek

α_1	parameter, Eqn. [3], s
β_1	parameter, Eqn. [3], Pa s
β_2	parameter, Eqn. [3], Pa s^2
δ	phase shift, degrees
ϕ	air volume fraction, -
ϕ_{max}	maximum air volume fraction,-
Φ	crowding factor, -
$\dot{\gamma}$	shear rate, s^{-1}
$\dot{\gamma}_R$	shear rate experienced at the rim of the parallel plates, s^{-1}
Γ	surface tension between liquid phase and the air, N m^{-1}
Γ_0	surface tension between the solvent and air, N m^{-1}
η_{app}	apparent viscosity, Pa s
η_0	zero-shear-rate viscosity, Pa s
η_r	relative viscosity, -
η'	real component of the complex viscosity, Pa s
η''	imaginary component of the complex viscosity, Pa s
$\lvert\eta^*\rvert$	magnitude of the complex viscosity, Pa s
λ	relaxation time, s
ρ_s	density, kg m^{-3}
ρ_{us}	density of deaerated sample, kg m^{-3}
τ	shear stress, Pa
τ^*	dimensionless shear stress, -
τ_{CR}^*	critical dimensionless shear stress, -
ω	angular frequency, Hz
Ω	rotational velocity, rad s^{-1}

Introduction

Bubbly liquids are dispersions of bubbles in a liquid, with bubble volume fractions typically ranging up to 50%. The continuous liquid phase is usually viscous, retarding coalescence and creaming. In the food sector, the bubble phase is usually air and aerated foods are ubiquitous, from beverages to baked products, ice creams, dairy systems and confectionery, *e.g*. Campbell and Mougeot (1999). Aeration yields a softer texture, increased spreadability, a more homogeneous appearance and a more uniform distribution of taste (Thakur *et al.*, 2003). Aerated foods are appreciated by the consumer for the particular texture that the air, entrapped as small cells, imparts to them. Moreover, air cells can be used to replace fats in low-calorie products and healthier foods (Gabriele *et al*., 2012). Bubbly liquids are also encountered in nature in the form of magmas (Manga and Loewenberg, 2001) and in other industrial sectors in the form of cement (Ahmed *et al*., 2009), extracted crude oil (Abivin *et al*., 2009), cosmetics and personal care products (Malysa and Lunkenheimer, 2008).

The presence of the bubble phase modifies the rheology of the liquid, giving rise to shear-thinning and viscoelastic behaviour. In steady shear, at low shear rates the bubbles resist deformation and the behaviour resembles that of suspensions, with relative viscosity increasing with bubble volume fraction, ϕ. At higher shear rates, bubble deformation occurs, promoting alignment with the flow and giving rise to shear-thinning. The transition to shear-thinning behaviour in bubbly liquids and emulsions is usually discussed in terms of the capillary number, *Ca*, which compares the deforming stresses from fluid shear to the restoring capillary pressure:

$$Ca = \frac{\eta_0 \dot{\gamma} r}{\Gamma} \qquad (1)$$

where η_o is the viscosity of the continuous liquid phase, $\dot{\gamma}$ is the imposed shear rate, r is the radius of the undeformed bubble, and Γ is the liquid-bubble interfacial tension. When *Ca* is large, the deforming force (given by the shear stress in the continuous phase, $\eta_o \dot{\gamma}$) is large compared to the restoring force (related to the capillary pressure in the bubble, $\sim 2\Gamma/r$), and the bubbles are deformed, resulting in shear-thinning. At high shear rates the relative viscosity, η_r (defined as the ratio of the

apparent viscosity of the aerated sample to the viscosity of the continuous phase), approaches the Voight average, 1-ϕ (Manga and Loewenberg, 2001). Experimental and modelling studies of shear flow and bubble shape interactions have been reported by several workers, *e.g*. Manga and Loewenberg (2001), Loewenberg and Hinch (1996), Thompson *et al.* (2001), and Müller-Fischer *et al.* (2008). Many of the studies in this area are principally concerned with emulsions: bubbly liquids represent a limiting case where the ratio of the viscosity of the dispersed phase to the continuous phase is small and where the large difference in densities allows the dispersed entities to change shape rapidly (*i.e*. little inertia).

Much of the prior work has considered isolated bubbles or dilute systems, whereas many bubbly liquids of interest involve moderate or high bubble loadings. Bubble crowding then affects the shear stress experienced by individual bubbles and workers such Golemanov *et al*. (2008) have advocated the use of the effective medium approach employed in dense suspensions to describe the shear stress in foams and concentrated emulsions. The capillary number is then replaced by the dimensionless shear stress, τ^*, defined as:

$$\tau^* = \frac{\tau}{\Gamma / r} \tag{2}$$

which for a single bubble in a Newtonian liquid is equivalent to *Ca*. Golemanov *et al*. reported a critical value for droplet break-up, τ_{CR}*, of ~0.40 for foams with $\phi \sim 0.92$ and a lower value of 0.15 for hexadecane-in-water emulsions with $0.83 < \phi < 0.95$. These values were orders of magnitude lower than those expected for single droplets in sheared Newtonian liquids.

Llewellin *et al*. (2002) provided a good review of the pertinent literature as part of their paper presenting a model for bubbly liquid rheology under steady and oscillatory shear conditions. They performed experiments using golden syrup as the continuous phase with air volume fractions up to 0.5 and reported bubble crowding effects in steady shear measurements. They also conducted oscillatory shear tests and reported noticeable viscoelastic effects arising from the presence of the bubble phase which could be described reasonably well by a modified linearized Frankel and

Acrivos model (Frankel and Acrivos 1970). They reported two forms of the model: (*i*) a monodisperse model, based on a single characteristic bubble size to account for all the bubbles in the liquid, and (*ii*) a polydisperse model, involving the bubble size distribution. The latter applies the monodisperse model to each bubble size fraction and calculates the overall response as the sum of the individual monodisperse contribution for each size classes weighted by the contribution of each size fraction to the total bubble volume fraction, ϕ.

In the Llewellin *et al*. model the real and imaginary parts of the complex viscosity, η' and η'', respectively, are given by:

$$\eta' = \frac{(\beta_1 + \alpha_1\beta_2\omega)}{1+\alpha_1^2\omega^2} \tag{3}$$

$$\eta'' = \frac{(\beta_1\alpha_1 - \beta_2)\omega}{1+\alpha_1^2\omega^2} \tag{4}$$

where ω is the angular frequency. The coefficient α_1 is calculated from

$$\alpha_1 = \frac{6}{5}\lambda\,, \tag{5}$$

where λ is the deformation time scale, given by

$$\lambda = K\left(\frac{\eta_0 r}{\Gamma}\right) \tag{6}$$

with K a dimensionless parameter (Loewenberg and Hinch, 1996). Parameters β_1 and β_2 are evaluated from

$$\beta_1 = b'\eta_0 \tag{7}$$

$$\beta_2 = \eta_0\alpha_1(1-\frac{5}{3}\varphi) \tag{8}$$

In fitting their oscillatory shear results to Equation [3-8], Llewellin *et al*. found that the data did not fit the form $b' = 1+\phi$ expected from the Frankel and Acrivos model. Their data fitted a linear relationship of the form $b' = 1+ a'\phi$, where a' is a constant. The oscillatory data reported here showed a similar linear dependency on ϕ. It should be noted that this model requires the continuous

126 phase to be Newtonian and equation [3] gives the steady state shear viscosity as the frequency
127 approaches zero.
128
129 All the above studies and the majority of others in this area have employed a Newtonian liquid as the
130 continuous phase. Many bubbly liquids of practical interest feature suspensions or solutions with
131 non-Newtonian behaviour as the continuous phase. The example which prompted the work reported
132 here is cake batter (*e.g*. Meza *et al*., 2011), where the continuous phase is primarily a suspension of
133 flour particles in a viscous sugar solution and ϕ ranges from 0.1 to 0.5. Chesterton *et al.* (2011a)
134 reported strongly shear-thinning behaviour and viscoelastic effects which could not be described
135 adequately by the existing literature. The influence of a non-Newtonian continuous phase has been
136 investigated to some extent in the related field of emulsions (*e.g*. Mabille, 2000) but the fundamental
137 understanding is currently incomplete.
138
139 The aim of this study is to quantify the influence of using a non-Newtonian, specifically a shear-
140 thinning, continuous phase in bubbly liquids and to provide data for future modelling studies. To this
141 effect, a systematic investigation of the rheological and structural behaviour of bubbly liquids with a
142 near-Newtonian viscous liquid (honey) and shear-thinning continuous phases has been performed.
143 The honey selected proved to have a measurable elastic component in oscillatory shear testing so is
144 not a purely Newtonian liquid but provides a close approximation. Measurable visco-elastic
145 behaviour has been reported previously for honeys by Witczak *et al.* (2011). Aqueous guar gum
146 solutions were used for the latter tests as these are widely used in food products (*e.g*. Miquelim and
147 Lannes, 2009) and gave an apparent viscosity at low shear rates similar to the honey (and the cake
148 batters studied by Chesterton *et al*., 2012). The shear-thinning liquid would ideally not introduce any
149 new rheological features but this is difficult to achieve in practice. The presence of guar gum in
150 concentrations between 0.15 and 1.0 wt% affects bubble size, increases the elasticity of the liquid
151 and contributes to a pseudo-solid behaviour (Chavez-Montes *et al*., 2004; Fernandez *et al*., 2007).
152
153 Both bubbly liquids were prepared by whisking in a planetary mixer, replicating many food
154 processing operations. The evolution of the structure of the systems was monitored by rheological

testing at steady shear and oscillatory shear as well as by image analysis. The role of surfactants on the properties of guar gum bubbly liquids was also studied. The results for the honey-based liquid are presented first, followed by those for the guar gum solutions. Similarities and differences are discussed.

Materials and Methods

Sample preparation

Commercial clear honey was obtained from a local supermarket (ASDA Pure Clear Honey). Aqueous solutions of 10 g/L guar gum were prepared following the procedure reported by Chenlo *et al*. (2010). The polymer was dispersed in tap water by stirring at 1400 rpm on a magnetic hotplate stirrer (VMS-C4 Advanced, VWR, UK) at room temperature overnight to ensure complete hydration of the guar gum. Some air was incorporated into the solution during stirring and deaerated samples of the continuous phase were obtained by centrifuging them at 2250 rpm (500*g*) for 5 min. The same protocol was used to prepare guar gum solutions containing surfactant (Tween 20, polyoxyethylene sorbitan monolaurate, Sigma-Aldrich, St. Louis, MO) at concentrations of 0.3, 1.0 and 2.0 mM. The latter concentrations lie above the measured critical micelle concentration (CMC) of the solutions (Figure 1).

Aeration of honey and guar gum solutions (with or without surfactant) was performed in a planetary-action mixer (Hobart N50-110, Hobart UK, London). Details of this mixer and the wall shear rates generated are reported in Chesterton *et al*. (2011b). The power input to the mixer was recorded using a Hameg model HM 8115-2 power meter (HAMEG Instruments, Kettering UK) connected to a datalogging PC and the power draw for mixing calculated by subtracting the power input measured for the mixer running at the same speed without any liquid present. The liquids were whisked for 1 to 10 minutes at a speed setting of 3, giving estimated wall shear rates of 500 s^{-1}. The air volume fraction increased with time, reaching $\phi \approx 0.40$ after 10 min. All samples were prepared at least in duplicate.

The air volume fraction, ϕ, was determined gravimetrically following the procedure reported by Allais *et al*. (2006). Measurements were performed at room temperature using a 150 mL plastic cup. The cup was filled with sample and the surface levelled using a spatula. The cup was then weighed and the density determined as the ratio of the mass of sample to cup volume. The air volume fraction was calculated from:

$$\phi = 1 - \frac{\rho_s}{\rho_{us}} \tag{9}$$

where ρ_s and ρ_{us} are the densities of aerated and unaerated samples, respectively. Measurements were made in triplicate.

Bubble size measurements

Estimates of the bubble size distributions were determined quantitatively using a Morphologi G3S image analysis system (Malvern Instruments Ltd., UK). Complementary information about bubble size, bubble size distribution, and behaviour under shear was obtained using a Linkam shear cell (Cambridge Shearing System, CSS, Cambridge, UK). Freshly prepared samples were placed between two microscope slides held 1 mm apart by plastic shims in the Morphologi unit and photographed at 10× magnification. Six consecutive and slightly overlapping images were taken, with the total view spanning two photographs in width and three photographs in height. The bubble size distribution was similar in each photograph. This arrangement minimised the number of partially viewed bubbles and maximised the area-to-perimeter ratio. Image processing was carried out semi-automatically: the diameter of each bubble was traced manually, and image analysis software (Corel Draw X3 Pro) used to measure the traced lines. The air bubbles were sufficiently dispersed to allow bubble diameters to be traced readily. Allais *et al*. (2006) employed a similar method and suggested a minimum of 250 measurements for accurate representation of an aerated sample. At least 250 bubbles were measured in each sample in this work. It should be noted that this technique does not give an exact bubble size distribution as the number of small bubbles obscured by larger ones is not known.

The bubble size data were grouped into classes following the protocol reported by Jakubczyk and Niranjan (2006), where the number of classes, N_c , and the class interval width, w, were given by:

$$N_C = \sqrt{n_b} \tag{10}$$

$$w = \frac{d_{\max} - d_{\min}}{N_C} \tag{11}$$

with n_b being the number of bubbles measured and d_{max} and d_{min} the smallest and largest measured bubble diameters, respectively. The bubble size data were evaluated by radius and were found to follow a log-normal distribution, as reported previously by Chesterton *et al*. (2012).

Rheological measurements

The majority of rheological measurements were carried out on a Bohlin CVO120HR controlled-stress rheometer (Malvern Instruments, Malvern, UK) using sand-blasted parallel plates (25 mm diameter and 1 mm gap) to prevent wall slippage. An ARES-LC controlled strain rheometer (TA Instruments Ltd., West Sussex, UK) was also used with either (*i*) parallel plates (50 mm diameter and 1 mm gap) with superfine sandpaper (mean asperity height 15 μm) attached to provide a rough surface, or (*ii*) Couette geometry (bob diameter 32 mm, cup diameter 34 mm, bob height 34 mm) with smooth walls. Measurements using the different tools showed only slight differences, indicating no contribution from slip effects.

Samples were loaded carefully to ensure minimal structural damage, and held at rest for 3 min before testing to allow stress relaxation and temperature equilibration. When using the parallel plate geometry a thin film of a Newtonian silicone oil (viscosity 1 Pa s) was applied to the exposed edge of the sample to prevent evaporation. Initial testing on a series of samples showed little difference between measurements made within 2 hours of sample preparation so all tests were conducted within this time frame. This result indicated that any phenomena such as coalescence and ripening which could change in the number and size of bubbles were not significant over this period. Samples for bubble size analysis were withdrawn shortly after the batter was prepared. Evolution of bubble size distribution due to ripening or coalescence was not monitored over this period. All measurements

were made under isothermal conditions (20ºC) and at least in duplicate. Error bars are plotted where the measurement uncertainty was greater than the symbols size.

Steady shear measurements

Viscous behaviour was studied using steady shear measurements. The apparent viscosity, η_{app}, was determined as function of shear rate, $\dot{\gamma}$, over the range of 0.1 to 500 s^{-1}, the upper limit being based on the estimated wall shear rate in the mixer. Hysteresis was studied by conducting increasing and decreasing shear rate sweeps up to different maximum shear rate values. Samples were sheared for 5 s at each shear rate in order to obtain steady-state. Since the shear rate varies with radial position in the parallel plate geometry, for the shear-thinning liquids the apparent viscosity data were calculated using (Steffe, 1996):

$$\eta_{app}(\dot{\gamma}_R) = \frac{T}{2\pi R_{pp}^3 \dot{\gamma}_R}\left(3 + \frac{d\ln T}{d\ln \dot{\gamma}_R}\right) \tag{12}$$

where $\dot{\gamma}_R$ is the shear rate evaluated at the rim, R_{pp} is the radius of the parallel plates and T is the torque reading.

The shear-thinning behaviour of guar gum solutions was fitted to the Cross-Williamson model (Cross, 1965):

$$\frac{\eta_{app}}{\eta_0} = \frac{1}{1 + k\dot{\gamma}^{(1-n)}} \tag{13}$$

where η_0 is the zero-shear rate viscosity, k is the time constant and n is the flow index.

Calculation of the dimensionless shear stress, τ^* (Equation [2]), requires knowledge of the interfacial tension, Γ. The surface tension between honey and air was taken from the literature (Llewellin *et al*. 2002) as 0.08 N m^{-1}. The surface tension between the guar gum solutions and air was determined experimentally using the sessile drop method with a Kruss Drop Shape Analyser 100 system. Values reported are the mean from at least ten measurements.

The normal force, F_{normal}, generated by the flow between plates was measured in steady shear tests on the Bohlin rheometer. Measurements of axial thrust were used to estimate the normal stress difference, N_1-N_2 via (Steffe, 1996):

$$N_1 - N_2 = \frac{2F_{normal}}{\pi R_{pp}^2}\left(1 + \frac{1}{2}\frac{d\ln F_{normal}}{d\ln \dot{\gamma}_R}\right) \quad (14)$$

The normal stress difference data were compared to the computed shear stress and apparent viscosity results to give an indication of when elastic forces became significant. The normal force correction due to inertial effects was estimated using (Kulicke *et al*., 1977)

$$F = -0.075\pi\rho_s\Omega^2 R_{pp}^4 \quad (15)$$

where Ω is the rotational velocity. This force correction was negligible for all tests conducted here.

Oscillatory shear measurements

Viscoelastic behaviour was investigated using small amplitude oscillatory shear testing. Strain sweeps (0.01-10%) were performed at 1 Hz prior to each frequency sweep in order to identify the region of linear viscoelasticity (LVE). Frequency sweeps were carried out over the range 0.1 to 10 Hz and back at a strain amplitude of 1%, well below the LVE limit, from which the storage modulus, G', loss modulus, G'', phase shift, δ, and magnitude of the complex dynamic viscosity, $|\eta^*|$, were determined.

Statistical analysis

Linear and nonlinear regressions were used to extract rheological parameters. The parameters of the models considered were determined from the experimental data with a one-factor analysis of variance (ANOVA) using PASW Statistics (v.18, IBM SPSS Statistics, New York, USA). When the analysis of variance indicated differences among means, a Duncan test was performed to differentiate means with 95% confidence ($p < 0.05$).

Results and Discussion

Surface tension

Figure 1 shows the results obtained for aqueous solutions with and without guar gum. The effect of surfactant concentration on surface tension was fitted to the Szyszkowski equation (Szyszkowski, 1908):

$$\frac{\Gamma}{\Gamma_0} = 1 - a\ln\left(1 + \frac{C}{b}\right) \tag{14}$$

where Γ_0 is the surface tension of the solvent, C is the concentration of the surfactant and a and b are fitting parameters. The data in Figure 1 indicate that the critical micelle concentration of the guar gum solutions with Tween 20 at 20°C lies near 0.4 mM, which is in reasonable agreement with the value of 0.17 mM for Tween 20 at 25ºC reported by Wu *et al.* (2006). The surface tension in the 1 wt% guar gum solutions was about 2 mN m^{-1} lower than that in water at the same surfactant concentration. These surface tension values were similar to those reported for aqueous guar gum dispersions by Moreira *et al*. (2012).

Bubbly liquids with viscous (near-Newtonian) continuous phase

Bubbly liquid preparation: honey

Bubbly liquids prepared with honey without surfactant were aerated for different periods (1, 2, 6 and 10 min). Table 1 shows that ϕ increased noticeably with mixing time. The ϕ values obtained after 6 and 10 min of aeration were not statistically different, with steady state values lying between 0.25 and 0.27. The instantaneous power draw due to mixing increased over the first couple of minutes from 127 W/kg to 146 W/kg as ϕ increased then reduced to an almost constant level (72 W/kg) after 6 min of aeration. Chesterton *et al*. (2012) used the same mixer to aerate cake batters and reported similar power draw behaviour.

Bubble size distribution: honey

Figure 2(*a*) shows a representative image of a honey-based bubbly liquid aerated for 10 min. The raw honey contained no bubbles, while images obtained after shorter aeration times showed similar

315 microstructure and marginally larger bubbles. The air volume fraction, ϕ, rose from 0.13 to 0.27 as
316 the aeration time increased from 1 to 10 min and this was accompanied by an increase in the number
317 of bubbles and a decrease in their mean radius (Table 1). After 6 min of aeration the total number of
318 bubbles increased very gradually, indicating that entrainment, break-up and disentrainment had
319 reached a steady state.
320
321 Honey aerated for 10 min contained bubbles with radii in the range 10-270 μm, which is larger than
322 the values reported for golden syrup by Llewellin *et al*. (2002), of 1-100 μm, using a different
323 mixing device (a Mondomix pin mixer operating at 1000 rpm). Figure 2(*b*) shows the bubble size
324 distribution obtained from optical microscopy, fitted to a log-normal distribution. The peak value
325 was around 40 μm, with a slightly higher value of 51 μm obtained with 1 and 2 min of aeration. All
326 the bubbly liquids studied, *i.e*. both those prepared with honey and with guar gum solutions,
327 exhibited similarly unimodal size distributions.
328
329

Steady shear measurements: honey

The honey was found to be Newtonian in steady shear tests, with a viscosity of 5 Pa s, whereas all bubbly liquids exhibited shear-thinning behaviour, where the apparent viscosity decreased with shear rate. Following the example of Golemanov *et al*. (2008), who argue that the effective medium approach is more relevant, the data are presented in Figure 3 as relative viscosity against the dimensionless shear stress (Equation [2]). The peak value of the bubble diameter in Figure 2 was used in the calculation of τ^*. The bubbly liquids all give $\eta_r > 1$ at low shear rates, which is expected since at low *Ca* or τ^* the system will behave as a suspension. At shear rates above 100 s^{-1}, the opposite trend is observed, with the bubbly liquid viscosity falling below that of the honey. This behaviour is consistent with the asymptotic limit previously reported for other Newtonian systems, *e.g*. alkyd resins/water emulsions (Thompson *et al*., 2001) and corn syrup bubbly liquids (Rust and Manga 2002). Our results show similar trends for each ϕ value:

(*i*) at small τ^*, < 0.01 or thereabouts, η_r is > 1, constant and sensitive to ϕ;

(*ii*) for $0.01 < \tau^* < 0.3$, η_r decreases with increasing τ^*; and

(iii) at $\tau^* > 0.3$, η_r is < 1 and approaches $1-\phi$.

Rust and Manga (2002) reported similar behaviour and fitted their data for bubbly corn syrup (ϕ = 0.163) in the shear-thinning region, (*ii*), to the empirical form

$$\eta_r = a_1 e^{-a_2 x} \qquad (17)$$

with the capillary number as the variable, *x*. This gave $a_1 = 1.2$ and $a_2 = 0.21$. We fitted our data to Equation [17] using τ^* rather than *Ca* as the variable and the plots in Figure 3 show reasonable agreement. The parameters a_1 and a_2 obtained by least-squares regression are given in Table 1. The a_1 and a_2 parameters are both noticeably larger than those reported by Rust and Manga.

The apparent viscosity at 1 s^{-1} was taken as an indicator of the low shear rate viscosity. This shear rate corresponded to $\tau^* < 0.01$ for each case and the bubbly liquid is expected to behave as a suspension. Plotting η_r against air volume fraction, ϕ, revealed a linear dependency described by $\eta_r = 1 + 7.4\phi$. (regression coefficient, $R^2 = 0.990$). Llewellin *et al*. reported a similar linear trend, of $\eta_r = 1 + 9.0\phi$, which is reasonably close to that found here.

358

359 Samples subjected to high shear rates were found to undergo microstructural changes. Figure 4
360 presents the behaviour observed with the bubbly liquid generated by aeration for 10 min. A series of
361 tests were performed, with shear rate sweeps from 0.1 s^{-1} up to 1, 10, 30, 100, and 300 s^{-1}, then back
362 to 0.1 s^{-1}. Three of the data sets are presented in the Figure. The increasing shear rate portion of each
363 test was repeated and the sample removed, photographed, and the air volume fraction measured as
364 before. The uncertainty in the ϕ values of the sheared samples was larger owing to the smaller
365 volume of sample available. Figure 2(*a*) shows a photograph of the bubbly liquid obtained after
366 mixing and before shearing. There were noticeable changes in the size and spatial distribution of the
367 bubbles following shearing. At 30 s^{-1} and higher shear rates, the return flow curve did not match
368 with the outgoing curve, indicating thixotropy, related to the bubbles changing during the tests. This
369 suggestion is supported by the images: above 30 s^{-1} there is a noticeable reduction in the size and
370 number of bubbles compared to those in the original sample. The measured air volume fraction was
371 smaller after subjecting the bubbly liquids to the higher shear rates than before. These observations
372 were confirmed by tests performed in the Linkam parallel-plates shear cell at the same shear rates as
373 in the Bohlin. Similar behaviour was also observed in tests in the ARES using a Couette cell,
374 indicating that it was not an artefact of the testing geometry. Vinckier *et al*. (1999) also observed
375 hysteresis in their samples, which was attributed to changing droplet size. Other workers such as
376 Rust and Manga (2002) did not report this thixotropic behaviour.
377

378 The flow curves at higher shear rates (Figure 4c) feature unexpected behaviour in that the bubbly
379 liquid exhibits a viscosity independent of shear rate on the return leg. The bubbly liquid still contains
380 a significant amount of air ($\phi \geq 0.20$) but the η_r values at a shear rate of 1 s^{-1} are noticeably close to
381 unity. Increasing the shear rate again gave similar results to those of the previous return leg,
382 indicating that the microstructure had not returned to its original state. This is an important result for
383 processing of these bubbly liquids as it suggests that the material remembers the highest shear rate
384 that it has been exposed to (at least over the time scale of these tests), *i.e*. significant thixotropy.
385

386 The normal stress difference data presented later in Figure 5 indicate that these bubbly liquids
387 generate appreciable elastic responses at higher shear rates. The associated change in hydrostatic
388 pressure is unlikely to cause a noticeable change in the amount of air dissolved in the continuous
389 phase. The mechanism by which the volume fraction of the sample decreases as well as the reason
390 the shear viscosity becomes independent of shear rate on the return leg should be investigated. These
391 observations illustrate the complexities introduced by the bubble phase and the challenges in
392 controlling the microstructure.
393
394 The plots of measured normal stress difference in Figure 5(*a*) show that N_1-N_2 for honey without
395 bubbles was practically negligible. For the bubbly liquids, however, N_1-N_2 increased rapidly at shear
396 rates above 1 s^{-1}, which corresponds to the onset of noticeable shear-thinning in Figure 3. Chesterton
397 *et al.* (2011a) also reported that the presence of the bubble phase gave rise to significant normal
398 forces in their study of cake batters, which were much larger than those associated with the
399 unaerated matrix. These results confirm that the bubble phase is responsible for the elastic effects.
400 The normal stress differences are also likely to cause bubble deformation and break-up, explaining
401 the changes in microstructure evident in Figure 4. The normal forces measured on the return leg in
402 tests such as those reported in Figure 4 were around 15-20% smaller than those measured on the
403 outward leg, which is consistent with the measured difference in air contents.
404
405 In their simulations of bubbly liquids at ϕ values up to 0.30, Loewenberg and Hinch (1996) predicted
406 the appearance of significant normal stress differences at higher *Ca*. They explained that large
407 normal stress differences can arise due to the reduced collision cross-section of the drops, which
408 allows them to glide past each other with less resistance and that elongation of the drops in the flow
409 direction produces large first normal differences. Their results suggest that the ratio N_1-N_2/τ should
410 approach unity at high *Ca* and this is seen with our data when replotted in this form in Figure 5(*b*).
411 Given that N_2 is normally small compared to N_1 ($N_2 \approx N_1/10$, according to Nielsen, 1977), the ratio
412 N_1-$N_2/\tau \approx N_1/\tau$. In steady shear, this is the ratio of the elastic to viscous forces, *i.e.* the Weissenberg
413 number, *Wi* (Poole, 2012). Figure 5(*b*) shows that this estimate of *Wi* approaches unity as the shear

414 rate increases but falls below unity at higher shear rates since N_1-N_2 approaches a plateau value of
415 around 500 Pa, while the shear stress continues to increase.
416
417 *Oscillatory shear measurements: honey*
418 The results above confirm that while elastic effects dominate the bulk rheology of wet and dry
419 foams, bubbly liquids with viscous liquids such as honey as the continuous phase have contributions
420 from both the bubble phase (elastic effects) and the continuous phase (viscous effects). Their
421 viscoelastic behaviour was investigated further, using small-strain oscillatory testing.
422
423 Selected mechanical spectra of honey and honey-based bubbly liquid obtained after 10 min aeration
424 are presented in Fig. 6. It is evident that $G'' > G'$ for both materials over the frequency range,
425 indicating predominantly viscous behaviour. The existence of a measurable, though small, elastic
426 component for the honey indicates that the material is not pure Newtonian, but 'weakly' viscoelastic:
427 stronger viscoelastic effects were reported for heather honeys by Witczak *et al*. (2011). Both data
428 sets show a strong frequency dependency, with both moduli increasing by two orders of magnitude
429 between 0.1 and 10 Hz. G'' is directly proportional to ω, as expected for Newtonian fluids. Addition
430 of air during 10 minutes of aeration increases both the viscous and elastic nature of the honey. The
431 values of G' and G'' for honey aerated for 1 min ($\phi = 0.13$) were not significantly different to those
432 for honey aerated for 2 min ($\phi = 0.14$) and lay between the data sets on Figure 6 (data not reported).
433 Similar trends were reported by Sahu and Niranjan (2009) for whipped cream, who noted that even
434 though the continuous phase may be purely viscous, bubble incorporation tends to make the
435 dispersion viscoelastic. Meza *et al*. (2011) reported that their cake batters showed significant elastic
436 behaviour with $G' \sim G''$, whereas here $G'' > G'$.
437
438 The relative importance of the viscous and elastic components is given by the phase shift, δ. The
439 elastic component of the bubbly liquids was measurable even at 0.1 Hz, and showed a pronounced
440 increase at the highest frequencies. The increase in the viscous modulus was not as large, so that the
441 ratio G''/G' (and hence δ) decreased with increasing frequency.

The above results for steady and oscillatory shear of honey-based bubbly liquids show similar behaviour to that reported for golden syrup-based bubbly liquids by Llewellin *et al*. (2002), so the data were fitted to the polydisperse form of their model based on the radius distribution (Equations [3-8]). The *b*' parameter values extracted from the oscillatory shear data (via Equation [7]) followed a linear dependency on ϕ, given by $b' = 1 + 1.15\phi$ ($R^2 = 0.993$), which is very close to the form $b' = 1 + \phi$ expected from Taylor's model (1932). In contrast, Llewellin *et al*. reported their data to fit the trend $b' = 1 + 9\phi$, but inspection in their paper suggests their data to belong to two groups, with *b*' values considerably lower than their reported trend for $\phi < 0.14$.

The difference between the mono- and poly-dispersed forms is illustrated with the data obtained for the 10 min bubbly liquid in Figure 7. The generalised polydisperse model based on the bubble radius distribution provided the best fit to the data, although it still shows some deviation from the measurements. These results demonstrate that bubble size distributions need to be measured (or aeration techniques which give monodispersed bubbles used). The phase shifts calculated with the polydisperse model showed good agreement with the experimental results (data not reported). Llewellin *et al*. also reported a minimum in phase shift (maximum in the elastic response) at about 1 Hz, which was related to the bubble size. This feature was not observed in these experiments.

The values of η_{app} at 1 s^{-1} (an estimate of the low-shear viscosity), *K* (from Equation [6]) and *b'* extracted by regression are presented in Table 1. There is a general trend of *K* increasing with increasing ϕ, as observed by Llewellin *et al*. (2002). The *K* values are in good agreement with those data previously reported by Llewellin *et al*. for bubbly liquids with similar ϕ values, whereas they are noticeably larger than the values obtained by Loewenberg & Hinch (1996) in their numerical calculations for emulsions in which the dispersed and continuous phases have the same viscosity.

Bubbly liquids with shear-thinning continuous phase

Bubbly liquid preparation: guar gum solutions

Samples were prepared with 10 g/L guar gum solution as the liquid phase in the same manner as the honey-based materials. The effect of surfactant was also studied. Figure 8(*a*) shows the effect of mixer speed setting on aeration in the absence of surfactant. Chesterton *et al*. (2011b) measured the orbital and planetary speeds and estimated the shear rate at the wall as (speed 1) 100-120 s^{-1}; (speed 2) 210-250 s^{-1}; (speed 3) 450-500 s^{-1}. The guar gum solution contained some bubbles initially ($\phi \sim$ 0.05) and there was no change in ϕ at speed setting 1, which was the value used in preparing the solution. At speed settings 2 and 3, ϕ increased noticeably over the first 2 minutes and approached a steady state value asymptotically. Figure 8(*a*) shows an almost linear relationship between air volume fraction and speed setting, with the highest ϕ values obtained at speed 3. Aeration at speed 3 for 10 min gave $\phi \sim 0.24$, which is close to that obtained with honey as the liquid phase under the same conditions.

The plots in Figure 8(*b*) show the effect of adding surfactant. There is a sharp initial rise in ϕ with mixing time, as noted above. Similar dynamics were observed with cake batters without emulsifier by Chesterton *et al*. (2012). As with honey, the mixer power consumption again showed an initial increase, followed by decrease to a steady state value. The lower absolute values (35 W/kg and 30 W/kg after 1 min and 4 min, respectively) despite the higher air content, indicates that the viscous resistance of the bubbly liquid with the shear-thinning liquid phase was lower than that of the honey mixtures even though the two liquids had similar low shear rate viscosities. The explanation lies in the shear-thinning nature of the guar gum solution.

The air fraction after a given mixing time increases with the concentration of surfactant. This is particularly noticeable in the solutions mixed for one minute. An analysis of the ϕ values (data not reported) showed that there was a small, but not statistically significant, difference in ϕ values for a given surfactant concentration after 4 min. There is a general increase in air content with surfactant concentration below the critical micelle concentration (CMC, about 0.4 mM, Figure 1). Above the

CMC, the increase in ϕ is modest. Similar behaviour was reported for other surface active agents present in espresso coffee (Piazza *et al*., 2008).

Bubble size distributions: guar gum solutions

Selected images for guar gum bubbly liquids aerated for 10 min without and with surfactant are presented in Figure 9(*a-d*). Bubbly liquids aerated for shorter times showed similar microstructures and marginally larger bubbles. Figure 9(*e*) shows that the fitted number size distributions were again unimodal and log-normal. Addition of surfactant resulted in larger air volume fractions and an increase in bubble size. After 10 min aeration without surfactant, the measured radii ranged from 35 to 357 μm, with a mode around 93 μm. With 2 mM surfactant, the radii range shifted to 80-580 μm, with a mode around 130 μm. All the guar gum solutions had distributions reflecting larger bubbles than those in honey (10-270 μm). The surface tension of the two liquids does not differ by more than a factor of 2 so this suggests that the bubbles in the guar gum solution experienced a lower deforming shear stress during mixing. Larger bubbles indicate that Γ/r is smaller and hence, if there is a critical value of *Ca* or τ^* for bubble break-up, the shear stress experienced by the bubbles must have been smaller. A lower shear stress is also consistent with the lower mixer power draw observed in preparing bubbly liquids with the guar gum solutions.

Steady shear measurements: guar gum solutions

Flow curves for centrifuged guar gum solution, as-prepared guar gum solution and the bubbly liquid generated by 10 min aeration in the absence of surfactant are shown in the form of shear rate sweeps in Figure 10. The continuous phase (centrifuged guar gum solution) exhibited apparent viscosity values at low shear rates close to those obtained for the honey. Unlike the honey, the centrifuged guar gum solution exhibits strong shear-thinning behaviour as reported elsewhere for guar gum solutions (Chenlo *et al*. 2010). They also reported a zero-shear rate limiting viscosity plateau at shear rates up to 10 s^{-1} but there is no evidence of this plateau in Figure 10 above 0.1 s^{-1}.

The guar gum solutions and their bubbly liquids all exhibited shear-thinning behaviour. The experimental data for guar gum samples in the absence of surfactant were satisfactorily fitted (R^2>

526 0.991, standard error < 0.047 Pa s) to the Cross-Williamson model, Eqn. [13], and the parameters η_0,
527 k and n obtained are summarised in Table 2. The η_0 values for the bubbly liquids were larger than
528 that of the guar gum solution, increasing with ϕ, which is analogous to suspension behaviour. The
529 variation in time constant with ϕ was modest, while the n values exhibited a decreasing trend with
530 increasing ϕ.
531
532 The bubbly liquids with the Newtonian liquid (honey) as continuous phase exhibited suspension-like
533 behaviour at low shear rates, with an almost linear dependency of the relative viscosity, η_r, at a shear
534 rate of 1 s^{-1}, on ϕ. The effect of air volume fraction on η_r for guar gum solutions, both with and
535 without surfactant, at different shear rates (0.1, 1.0 and 100 s^{-1}) is presented in Figure 11. The
536 relative viscosity was calculated by dividing the measured apparent viscosity by that measured for
537 the centrifuged guar gum solution at the same shear rate. At 0.1 and 1.0 s^{-1}, η_r increases with ϕ, in a
538 similar manner, while at 100 s^{-1}, η_r first increases with ϕ (in the bubbly liquids without surfactant),
539 and then decreases with ϕ (in the bubbly liquids with surfactant). The increase in η_r at the lower
540 shear rates is noticeably smaller than that observed with the near-Newtonian liquid phase. For $\phi >$
541 0.25, *i.e.* those containing surfactant, the trend weakens. At 100 s^{-1}, η_r increases only modestly with
542 ϕ and is < 1 at higher ϕ, indicating strongly non-Newtonian, shear thinning, behaviour.
543
544 Figure 12(*a*) shows a series of flow curves (presented as η_r) for the guar gum solution and bubbly
545 liquids prepared from it by adding various amounts of surfactant and then mixing for 10 minutes.
546 The profiles are similar to the honey-based bubbly liquids (Figure 3), decreasing steadily from high
547 to low viscosity as the shear rate increases. Unlike the honey-based bubbly liquids, the η_r values for
548 the guar gum-based bubbly liquids fall below 1 and approach (1- ϕ) only at the highest surfactant
549 content.
550
551 Plotting η_r for the bubbly liquids with ϕ between 0.24 and 0.38 against the dimensionless shear
552 stress in Figure 12(*b*) shows that the data sets pass through a common point ($\eta_r \sim 1.25$ at $\tau^* \sim 0.03$-
553 0.04), suggesting that this is a critical value of the dimensionless shear stress. That for $\phi = 0.39$

554 passes through the point and rapidly approaches the Voight limit. Similar behaviour was observed
555 for the honey-based bubbly liquids in Figure 3 but with convergence at $\tau^* \sim 0.3$, *i.e.* an order of
556 magnitude greater than with the shear-thinning continuous phase here. This result suggests that the
557 microstructural changes responsible for the reduction in shear viscosity occur at significantly lower
558 shear rates in the guar gum-based bubbly liquids than in the honey-based bubbly liquids, which is
559 consistent with the observations of larger bubble sizes and smaller power draw values for the shear-
560 thinning continuous phase.
561
562 The effect of shear rate on bubble structure was investigated with a guar gum solution containing 0.3
563 mM surfactant aerated for 10 min as this had a bubble volume fraction of 0.28, which was similar to
564 the honey-based bubbly liquid for which results are presented in Figure 4. Figure 13 shows evidence
565 of thixotropy in these guar gum-based bubbly liquid even at the lowest value of the maximum shear
566 rate (1 s^{-1}), with noticeable differences in the flow curves for increasing and decreasing shear rates.
567 Even after being sheared to 100 s^{-1} and 300 s^{-1} the return sweeps showed evidence of shear-thinning.
568 The relative viscosity is lower in the return sweep and drops below unity on both the forward and the
569 return sweeps, especially when the maximum shear rate is large. The changes in bubble size and
570 content were confirmed by Linkam measurements.
571
572 This behaviour differs from the honey-based bubbly liquids, where differences in the flow curves
573 were not apparent until the shear rate on the outward ramp reached 30 s^{-1}. Differences between the
574 initial and the final volume fraction of bubbles were also evident at smaller maximum shear rates for
575 the guar gum-based bubbly liquids. The return leg in the honey-based liquid showed constant
576 viscosity, while those in guar gum exhibited weaker shear-thinning behaviour than the outward leg.
577
578 The normal stress differences in Figure 14(*a*) can be usefully compared with the estimate of the
579 shear stress, τ, required to deform a bubble (given by Γ/r: this is equivalent to finding τ such that τ^*
580 =1) For the guar gum solution without surfactant this gives $\tau \sim 0.07$ N/m/(9.3×10^{-5} m) = 750 Pa,
581 and the N_1-N_2 values for the as-prepared guar gum solution ($\phi = 0.05$) only approach this value at the
582 highest shear rates, explaining why its relative viscosity in Figure 12 decreases modestly and does

583 not approach unity. For all the bubbly liquids, however, the N_1-N_2 values reach the corresponding
584 Γ/r value at moderate shear rates. The shear rates at which N_1-$N_2 \sim \Gamma/r$ are summarised in Figure
585 14(*b*), and confirm that bubble deformation is likely to occur both during mixing and the steady
586 shear flow curve tests.
587
588 Figure 14(*c*) compares the ratio of the measured normal stress difference to the shear stress at a shear
589 rate of 100 s^{-1}, which is at the lower end of the range of wall shear rates generated in the mixer. The
590 ratio of stresses is always > 10 and exceeds 200 at the highest ϕ values, indicating that at all ϕ, but
591 especially at high ϕ, the wall shear rates generated in the mixer are likely to cause bubble break-up
592 via elastic deformation. The data exhibit three regions, namely (*i*) no surfactant, $\phi < 0.24$, (*ii*) $0.24 <$
593 $\phi < 0.39$, where the surfactant concentration is below the CMC, and (iii) $\phi > 0.39$, high surfactant
594 concentration. The role played by the surfactant and mixer shear rate in determining the number and
595 size distribution of the bubbles, and hence the bubbly liquid rheology, requires further work.
596
597 Finally, Figure 14(*d*) shows the data in Figure 14(*a*) plotted in the form of the approximate
598 Weissenberg number against the dimensionless shear stress. The data sets follow a similar pattern,
599 reaching *Wi* values of order 10^3 at dimensionless shear stress values < 0.1. We are not aware of
600 prior work in the literature on bubbly liquids considering bubble deformation and break-up under
601 the combination of shear and normal stresses generated in these liquids, but it is expected to differ
602 from that reported for Newtonian liquids as the stress field is highly anisotropic even under
603 notionally steady shear conditions. Mabille (2000) reported that emulsions prepared with a shear-
604 thinning continuous phase gave larger droplets than a Newtonian liquid with the same apparent
605 viscosity, but no explanation was offered. Extending the simulation studies of Loewenberg and
606 Hinch (1996) to consider shear-thinning liquids, for instance, would allow us to determine whether
607 the large *Wi* values in Figure 14(*d*) arise from the presence of the bubble phase alone or from it
608 augmenting the elasticity of the guar gum solutions. The importance of the topic lies in its
609 application in manufacturing structured products: Chesterton *et al*. (2012) reported behaviour in their
610 study of cake batters. In that case, the shear-thinning nature of the continuous phase plays an

611 essential role in giving a high apparent viscosity after bubbles are generated in the mixer, retarding
612 subsequent creaming of the bubbles in the batter.
613
614 *Oscillatory shear measurements: guar gum solutions*
615 The sizeable elastic effects observed in the steady shear tests highlight the need for small amplitude
616 oscillatory testing to probe the behaviour of these bubbly liquids. The protocols used with the guar
617 gum based samples were identical to those used for the honey-based samples. Mechanical spectra
618 (G' and G'' vs. angular frequency) of centrifuged guar gum solution and bubbly liquids aerated for 10
619 min without and with surfactant (2.0 mM) are presented in Figure 15. The mechanical behaviour for
620 the centrifuged gum solutions was dependent on frequency and follows the shape reported elsewhere
621 for similar gum solutions (Steffe, 1996; Chenlo *et al*. 2010). Both moduli increased with frequency,
622 with $G''>G'$ at low frequencies, and $G'>G''$ at high frequencies, confirming that the guar gum
623 solution had a significant larger elastic component than honey (compare with the honey spectra in
624 Figure 6). The presence of air bubbles increased both moduli, with both the low frequency value
625 (dominated by viscous flow) and high frequency value (dominated by bubble elasticity) increasing
626 with ϕ. For the bubbly liquid without surfactant and $\phi = 0.24$ (Figure 15(*a*)), both moduli increased
627 roughly 5-fold at low frequency and the crossover frequency was shifted from 4 down to 2 Hz. With
628 2 mM surfactant ($\phi = 0.39$, Figure 15(*b*)), however, the storage modulus increased 13-fold at 0.02 Hz
629 and was significantly larger than the loss modulus of the centrifuged solution. The crossover
630 frequency also decreased further, to 0.4 Hz.
631
632 Comparing samples with similar ϕ values showed similar values of G' and G'', with no statistically
633 significant effect of surfactant content. It was not possible to fit the Llewellin *et al*. model to these
634 data sets.
635
636 Newtonian and non-Newtonian liquid phases: similarities and differences
637 The above results confirm that the rheology and processing of a bubbly liquid is intimately related to
638 the nature of the continuous phase as well as the bubble volume fraction and bubble behaviour. The
639 bubbly liquid based on guar gum solutions exhibits qualitatively similar behaviour to that observed

with the honey, but at different shear rates. Bubble crowding as discussed by Golemanov *et al*. (2008) is important in both cases, but the value of the dimensionless shear stress at which noticeable bubble deformation (and the onset of shear-thinning) occurs for the guar gum solutions is smaller.

Normal stress differences play an important role in the onset of shear-thinning. Sizeable N_1-N_2 values are generated in the unaerated guar gum solutions (as stated in the Introduction, it is difficult to find a purely shear-thinning fluid) and these are enhanced by the presence of bubbles. N_1-N_2 values large enough to cause bubble deformation and shear-thinning were therefore observed at lower shear rates, and dimensionless shear stresses, in the guar gum solutions.

Even though both types of bubbly liquid were mixed using the same device and procedure, and entrained similar volume fractions of air, the bubbles in the honey were noticeably smaller than those in the shear-thinning liquid. The difference in bubble sizes could not be explained by differences in surface tension. The explanation supported by the data presented here is that the shear stresses experienced by the bubbles at the high shear rates produced by the mixer were larger in the Newtonian liquid than in the shear-thinning liquid, which, when combined with the sizeable normal stresses, made it easier to overcome the surface tension of the bubbles and break them up.

Addition of surfactant to the shear-thinning liquid made it possible to increase the air volume fraction (also termed holdup), which was accompanied by larger entrained bubbles. These larger bubbles could, in turn, be deformed and broken up more readily. Detailed examination of absolute numbers of bubbles per unit volume over time, as reported by Chesterton *et al*. (2012), is needed to determine the effect of surfactant on bubble entrainment and breakup.

Summary and Conclusions

Bubbly liquids made from a near-Newtonian liquid (honey) and a shear-thinning liquid (solutions of guar gum) with a low-shear viscosity close to that of the honey both exhibited shear-thinning behaviour and large normal stress differences as a result of the presence of the bubble phase.

The behaviour of the honey-based liquids exhibited many of the features reported by previous experimental and simulation studies, including the development of high normal stress differences and relative shear viscosity approaching the Voight limit at higher shear rates. Crowding effects, reported for emulsions, are also found to be significant in bubbly liquids. The shear rates at which the normal stress difference approached the capillary pressure corresponded to the onset of shear-thinning behaviour, indicating that the elasticity introduced by the bubble phase contributes significantly to bubble deformation. At shear rates where bubble deformation occurs, the observation of constant shear viscosity (accompanied by decreasing normal stress differences) as the shear rate decreases has not been reported and deserves further attention as it suggests a memory effect.

The unaerated shear-thinning liquid exhibited normal stress differences and elastic effects which were enhanced by the presence of the bubbles. The bubbly liquids prepared with the shear-thinning liquid also exhibited a decrease in the volume fraction and a diminution of their shear-thinning character when subjected to high shear rates. The plots of relative viscosity versus dimensionless shear stress for the guar gum bubbly liquids also seemed to cross at a common point, which was lower than that for honey and those reported for Newtonian liquid emulsions by Golemanov *et al*. (2008). The normal stress differences generated in the shear-thinning liquid were much larger than those generated in the near-Newtonian viscous liquid, and the onset of shear-thinning again corresponded to the shear rate at which the stress difference approached the estimated capillary pressure. Surfactant allowed more air to be whisked into the liquid, but gave larger bubble sizes which were subsequently easier to deform: with the guar gum bubbly liquids only those prepared with high surfactant concentration exhibited an apparent shear viscosity approaching the Voight limit.

Acknowledgements

The authors acknowledge the financial support from Spain's Ministerio de Educación. We also wish to thank Tao Wang for his assistance with the surface tension measurements and Drs Simon Butler, Amy Chesterton and Min Zhang for their help with the experiments.

References

Abivin P, IHenaut I, Argillier J-F, Moan M (2009) Rheological behavior of foamy oils, Energy & Fuels, 23, 1316–1322.

Ahmed RM, Takach NE, Khan UM, Taoutaou S, James S, Saasen A, Godøy R (2009) Rheology of foamed cement, Cement and Concrete Research, 39, 353–361.

Allais I, Edoura-Gaena RB, Gros JB, Trystram G (2006) Influence of egg type, pressure and mode of incorporation on density and bubble distribution of a lady finger batter. Journal of Food Engineering, 74, 198-210.

Campbell GM, Mougeot E (1999) Creation and characterisation of aerated food products, Trends in Food Science and Technology, 10, 283-296.

Chavez-Montes BE, Choplin L, Schaer E (2007) Rheological characterization of wet food foams. Journal of Texture Studies 38, 236–252.

Chenlo F, Moreira R, Silva C (2010) Rheological properties of aqueous dispersions of tragacanth and guar gums at different concentrations. Journal of Texture Studies, 41, 396-415.

Chesterton AKS, Meza BE, Moggridge GD, Sadd PA, Wilson DI (2011a) Rheological characterisation of cake batters generated by planetary mixing: elastic versus viscous effects. Journal of Food Engineering, 105, 332-342.

Chesterton AKS, Moggridge GD, Sadd PA, Wilson DI (2011b) Modelling of shear rate distribution in two planetary mixtures for studying development of cake batter structure. Journal of Food Engineering, 105, 343-350.

Chesterton AKS, Pereira de Abreu, DA, Moggridge GD, Sadd PA, Wilson DI (2012) Evolution of cake batter bubble structure and rheology during planetary mixing, Food and Bioproducts Processing, in press.

Cross MM (1965) Rheology of non-Newtonian fluids: a new flow equation for pseudoplastic systems. Journal of Colloid Science, 20, 417-437.

Fernandez PP, Martino MN, Zaritsky NE, Guignon B, Sanz PD (2007) Effects of locust bean, xanthan and guar gums on the ice crystals of a sucrose solution frozen at high pressure. Food Hydrocolloids, 21, 507-515.

Frankel NA, Acrivos A (1970) The constitutive equation for a dilute emulsion. Journal of Fluid Mechanics, 44, 65-78.

Gabriele D, Baldino N, Migliori M, de Cindio B, Tricarico C (2012) Modelling flow behaviour of dairy foams through a nozzle. Journal of Food Engineering, 109, 218-229.

Genovese DB, Lozano JE, Rao MA (2007) The rheology of colloidal and noncolloidal food dispersions. Journal of Food Science, 72, R11-R20.

Golemanov K, Tcholakova S, Denkov ND, Ananthapadmanabhan KP, Lips A (2008) Breakup of bubbles and drops in steadily sheared foams and concentrated emulsions. Physical Review E, 78, 051405-1-051405-12.

735 Jakubczyk E, Niranjan K (2006) Transient development of whipped cream properties. Journal of
736 Food Engineering, 77, 79-83.
737 Llewellin EW, Mader HM, Wilson SDR (2002) The rheology of a bubbly liquid. Proceedings of the
738 Royal Society of London Series A-Mathematical Physical and Engineering Sciences, 458,
739 987-1016.
740 Loewenberg M, Hinch J (1996) Numerical simulation of a concentrated emulsion in shear flow.
741 Journal of Fluid Mechanics, 321, 395-419.
742 Kulicke WM, Kiss G, Porter RS (1977) Intertial normal-force corrections in rotational geometry,
743 Rheologica Acta, 16, 568-572.
744 Mabille, C. (2000) Fragmentation in emulsions submitted to a simple shear, PhD Dissertation,
745 Bordeaux I University, cited in Leal-Calderon,. F. (and co-authors) (2007) *Emulsion Science:*
746 *Basic Principles*, 2nd edition, Springer, Chapter 1.
747 Malysa K, Lunkenheimer K (2008) Foams under dynamic conditions. Current Opinion in Colloid
748 and Interface Science, 13, 150-62.
749 Manga M, Loewenberg M (2001) Viscosity of magmas containing highly deformable bubbles.
750 Journal of Volcanology and Geothermal Research, 105, 19-24.
751 Meza BE, Chesterton AKS, Verdini RA, Rubiolo AC, Sadd PA, Moggridge GD, Wilson DI (2011)
752 Rheological characterisation of cake batters generated by planetary mixing: Comparison
753 between untreated and heat-treated wheat flours. Journal of Food Engineering, 104, 592-602.
754 Miquelim JN, Lannes, SCDS (2009) Egg albumin and guar gum influence on foam thixotropy.
755 Journal of Texture Studies, 40, 623-636.
756 Moreira R, Chenlo F, Silva C, Torres MD, Díaz-Varela D, Hilliou L, Argence H (2012) Surface
757 tension and refractive index of guar and tragacanth gums aqueous dispersions at different
758 polymer concentrations, polymer ratios and temperatures. Food Hydrocolloids, 28, 284-290.
759 Müller-Fischer N, Tobler P, Dressler M, Fischer P, Windhab EJ (2008) Single bubble deformation
760 and breakup in simple shear flow. Experiments in Fluids, 45, 917-926.
761 Nielsen, L. E. (1977) *Polymer Rheology*, New York, Marcel Dekker.
762 Piazza L, Gigli J, Bulbarello A (2008) Interfacial rheology study of espresso coffee foam structure
763 and properties. Journal of Food Engineering, 84, 420-429.
764 Poole, R (2012) The Deborah and Weissenberg numbers, British Society of Rheology Bulletin,
765 53(2), 32-38.
766 Rust AC, Manga M (2002) Effects of bubble deformation on the viscosity of dilute suspensions.
767 Journal of Non-Newtonian Fluid Mechanics, 104, 53-63.
768 Sahu JK, Niranjan K (2009) Gas-liquid mixing. In Cullen, P. J. (Ed.) *Food Mixing: Principles and*
769 *Applications*. Wiley-Blackwell.
770 Steffe JF (1996) *Rheological Methods in Food Process Engineering*, Freeman Press.
771 Szyszkowski B (1908) Experimentelle Studien über kapillare Eigenschaften der wässrigen Lösungen
772 von Fettsäuren, Zeitschrift für Physikalische Chemie, 64, 385-414.

773 Taylor GI (1932) Viscosity of a fluid containing small drops of another fluid, Proc. Royal Society of
774 London, A138, 41–48.
775 Thakur RK, Vial Ch, Djelveh G (2003) Influence of operating conditions and impeller design on the
776 continuous manufacturing of food foams. Journal of Food Engineering, 60, 9-20.
777 Thompson MJ, Pearson JRA, Mackley MR (2001) The effect of droplet extension on the rheology of
778 emulsions of water in alkyd resin. Journal of Rheology, 45, 1341-1358.
779 Vinckier I, Minale M, Mewis J, Moldenaers P (1999) Rheology of semi-dilute emulsions:
780 viscoelastic effects caused by the interfacial tension. Colloids and Surfaces A, 150, 217-228.
781 Wang, T., Davidson, J.F. and Wilson, D.I. (2013) Effect of surfactant on flow patterns and draining
782 films created by a horizontal liquid jet impinging on a vertical surface, Chemical Engineering
783 Science, 88, 79-94.
784 Witczak M, Juszczak L, Galkowska D (2011) Non-Newtonian behaviour of heather honey, Journal
785 of Food Engineering. 104, 532-537.
786 Wu, D., Xu, G.Y., Liu, J. and Li, Y.M. (2006) Investigation on adsorption dynamics of
787 protein/Tween-20 mixture at the surface of solution by surface pressure measurement, J.
788 Dispersion Sci. Tech., 27: 523-526.
789

Figure Captions

Figure 1 Effect of surfactant concentration on surface tension relative to water. Data for Tween 20 in water taken from Wang *et al.* (2013). Symbols: closed circles – water with surfactant, open diamonds – guar gum with surfactant. Solid trend line shows Equation [14] fitted to the Tween 20data with parameters a = 0.09 and $b = 3.3\times10^{-6}$ M. Experimental data showed high reproducibility and estimated uncertainty is smaller than symbol size.

Figure 2 Honey-based bubbly liquid generated after 10 min aeration. (*a*) optical microscope image; (*b*) bubble number distribution. Solid line shows log-normal distribution fitted to data set with parameters: mean, 40 μm; standard deviation of *ln*(diameter), 0.383.

Figure 3 Data for honey-based liquids plotted in the form of relative viscosity as a function of the dimensionless shear stress, τ^*. Solid line – honey; open symbols - bubbly liquids. Air volume fraction values are shown in parenthesis for each data set. Loci show fits to Equation [17], with parameters given in Table 1. In this and subsequent plots, error bars are not plotted if the uncertainty in data values is smaller than the symbol size.

Figure 4 Honey bubbly liquid (10 min aeration) (*i*) flow curves with increasing and then decreasing shear rates and (*ii*) photomicrographs of samples removed at time P, after a maximum shear rate of (*a*): 1 s^{-1}, (b): 30 s^{-1}, and (c): 300 s^{-1}. Symbols: open circles –measurements at increasing shear rate, closed circles –measurements at decreasing shear rate. Air volume fraction values shown in parentheses correspond to those before and after tests. Figure 2(*a*) shows the bubbly liquid before testing.

Figure 5 Normal and shear stress parameters obtained for honey bubbly liquids: (*a*) normal stress difference (N_1-N_2), and (*b*) ratio of the measured normal stress difference to shear stress. Solid symbols – honey; open symbols – bubbly liquids. Air volume fraction values are shown in parenthesis for each data set. Dashed locus in (*a*) shows normal stress from inertial effects calculated for honey using Equation [16].

Figure 6 Dynamic mechanical spectra of honey and bubbly liquids: loss and storage moduli as function of the frequency of oscillation. ϕ values shown in parentheses for each data set.

Figure 7 Comparison of the fit of the monodispersed (solid lines) and polydispersed (dashed lines) forms of the Llewellin *et al*. model to the complex viscosity measured for the honey-based bubbly liquid after 10 min aeration. Solid symbols – honey; open circles – bubbly liquid. Liquid air volume fractions shown in parentheses.

Figure 8 Effect on the air volume fraction of 1 wt% aqueous guar gum solutions of (*a*) mixer speed setting in the absence of surfactant, and (*b*) surfactant concentration at mixer speed 3. Closed symbols – guar gum solution, open – bubbly liquids.

Figure 9 Bubbly liquids prepared with 1.0% w/w guar gum, 10 min aeration: (*a*) without surfactant, and with (*b*) 0.3, (*c*) 1.0, (*d*) 2.0 mM Tween 20. Bubble number size distributions in (*e*) show log-normal fits based on the radii. ϕ values given in parentheses.

Figure 10 Flow curves of surfactant-free guar gum solution and bubbly liquids made with guar gum (1.0%, w/w) after different mixing times. Solid symbols - centrifuged solution, open symbols - bubbly liquids (guar gum solution, circles; 10 min aeration, squares). The solid line shows the best fit to the centrifuged solution obtained with the Cross model (Equation [13]). Air volume fraction values are shown in parentheses for each data set.

Figure 11 Effect of air volume fraction on guar gum bubbly liquid relative viscosity at shear rates of 0.1, 1.0 and 100 s^{-1}. Solid line shows linear trend line obtained by regression for honey, with $\eta_r = 1 + 7.4\phi$ ($R^2 = 0.990$).

Figure 12 Relative viscosity of guar gum solutions with surfactant (0.3, 1.0 and 2.0 mM) as a function of (*a*) shear rate and, (*b*) τ^*. Air volume fraction values are shown in parentheses.

Figure 13 Guar gum bubbly liquids prepared with 0.3 mM surfactant and 10 min aeration: (*i*) flow curves for increasing and then decreasing shear rates; (*ii*) images taken after shearing to a maximum shear rate of (*a*) 1 s^{-1}; (b) 30 s^{-1}; (c) 300 s^{-1}. Figure 9(*b*) shows a photograph of the bubbly liquid before testing. Symbols: open circles – measurements at increasing shear rates, closed circles – measurements at decreasing shear rates. Air volume fraction values for each data set are shown in parentheses. Point P – time at which sample was removed and photograph taken.

Figure 14 Stress parameters measured for guar gum solutions and bubbly liquids with and without surfactant: (*a*) N_1-N_2, and (*b*) shear rate at which N_1-$N_2 \approx \Gamma/r$; (c) ratio of the measured normal stress difference to shear stress at 100 s^{-1} (marked with a vertical line in (*a*)) at different air volume fractions;(d) estimated Weissenberg number (= (N_1-N_2)/τ) plotted against dimensionless shear stress. ϕ values shown in parentheses for each data set.

Figure 15 Mechanical spectra of centrifuged 1 wt% guar gum solution and bubbly liquids generated by 10 min aeration (*a*) without and (*b*) with 2.0 mM of surfactant. Symbols: closed – centrifuged guar gum solution, open – bubbly liquids. Air volume fraction values shown in parentheses for each data set.

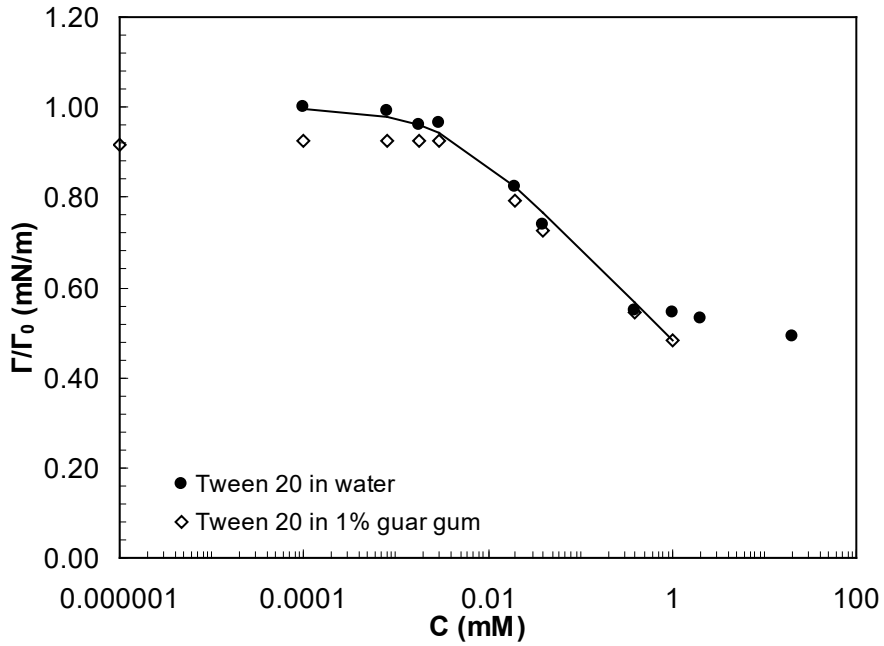

868
869

870 **Figure 1** Effect of surfactant concentration on surface tension relative to that of water. Data for
871 Tween 20 in water taken from Wang *et al.* (2013). Symbols: closed circles – water with
872 surfactant, open diamonds – guar gum with surfactant. Solid trend line shows Equation [14]
873 fitted to the Tween 20 data with parameters $a = 0.09$ and $b = 3.3\times10^{-6}$ M. Experimental
874 data showed high reproducibility and estimated uncertainty is smaller than symbol size.

(*a*)

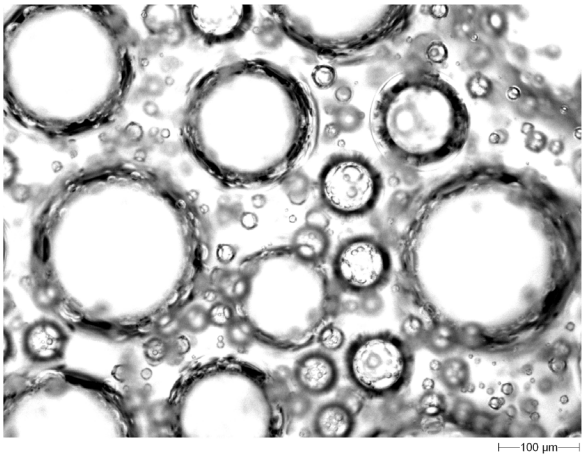

(*b*)

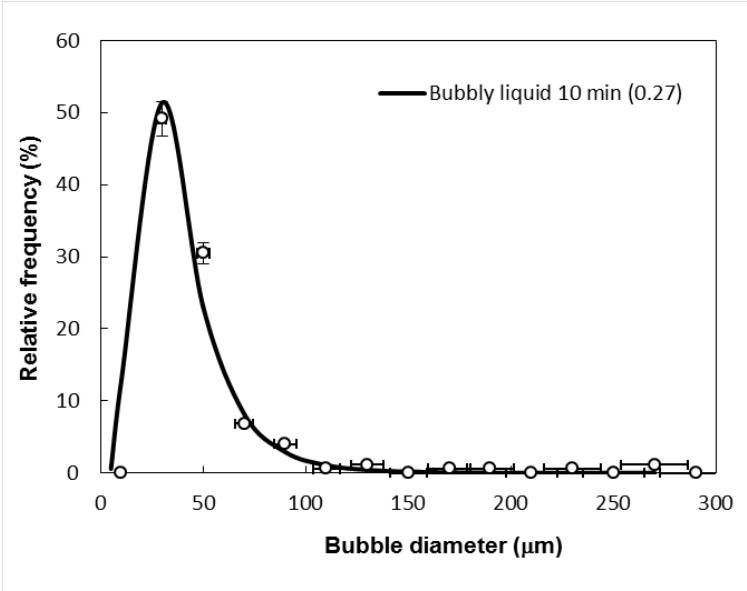

Figure 2 Honey-based bubbly liquid generated after 10 min aeration. (*a*) optical microscope image; (*b*) bubble number distribution. Solid line shows log-normal distribution fitted to data set with parameters: mean, 40 µm; standard deviation of *ln*(diameter), 0.383.

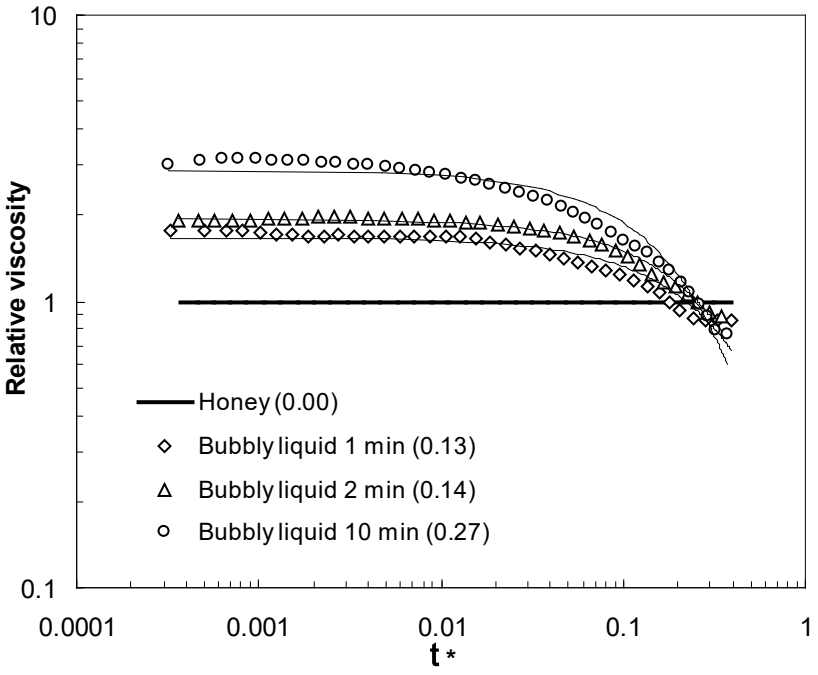

884

885

886

887 **Figure 3** Data for honey-based liquids plotted in the form of relative viscosity as a function of the
888 dimensionless shear stress, τ^*, for increasing shear rate tests. Solid line – honey; open
889 symbols - bubbly liquids. Air volume fraction values are shown in parenthesis for each data
890 set. Loci show fits to Equation [17], with parameters given in Table 1. In this and
891 subsequent plots, error bars are not plotted if the uncertainty in data values is smaller than
892 the symbol size.

893

(*i*) (*ii*)

(*a*)

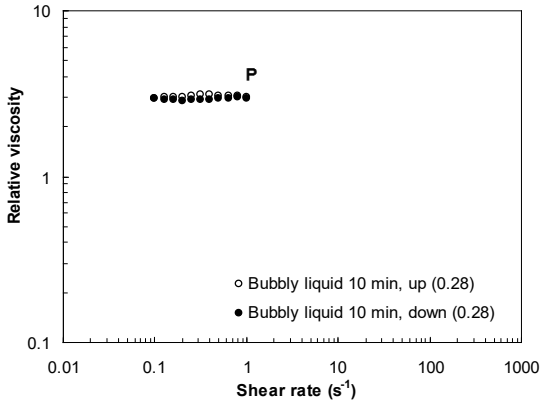

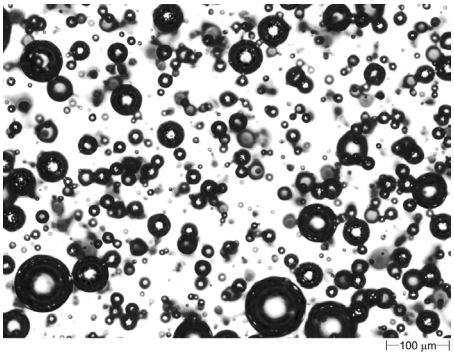

(b)

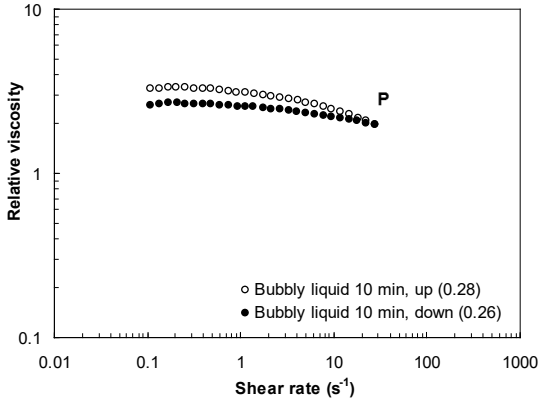

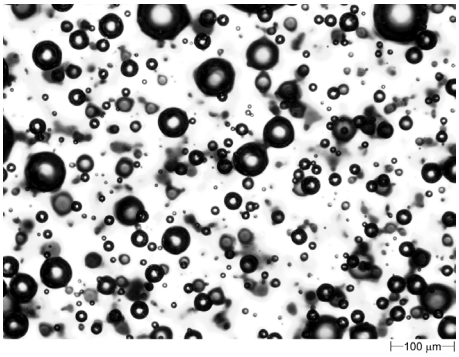

(*c*)

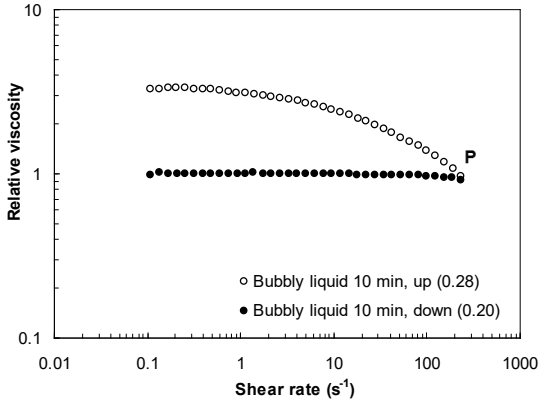

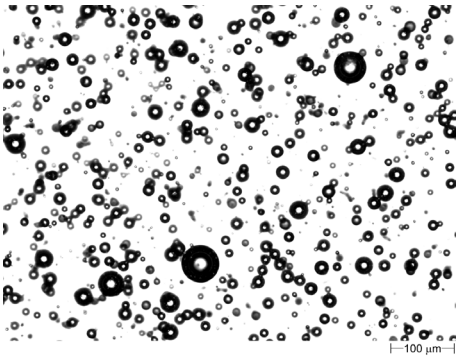

Figure 4 Honey bubbly liquid (10 min aeration) (*i*) flow curves with increasing and then decreasing shear rates and (*ii*) photomicrographs of samples removed at time P, after a maximum shear rate of (*a*): 1 s^{-1}, (b): 30 s^{-1}, and (c): 300 s^{-1}. Symbols: open circles –measurements at increasing shear rate, closed circles –measurements at decreasing shear rate. Air volume fraction values shown in parentheses correspond to those before and after tests. Figure 2(*a*) shows the bubbly liquid before testing.

908 (a)

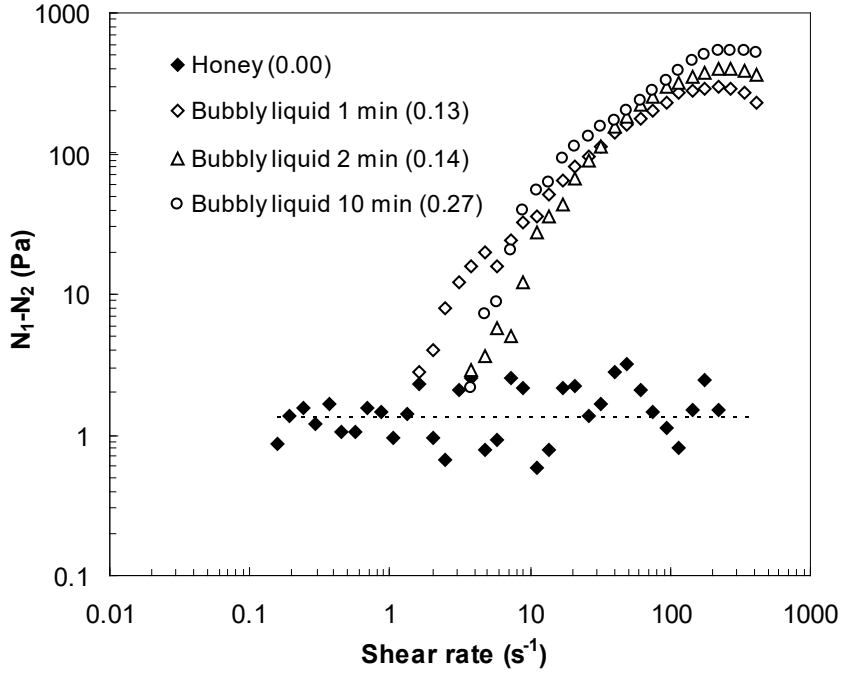

909
910 (b)

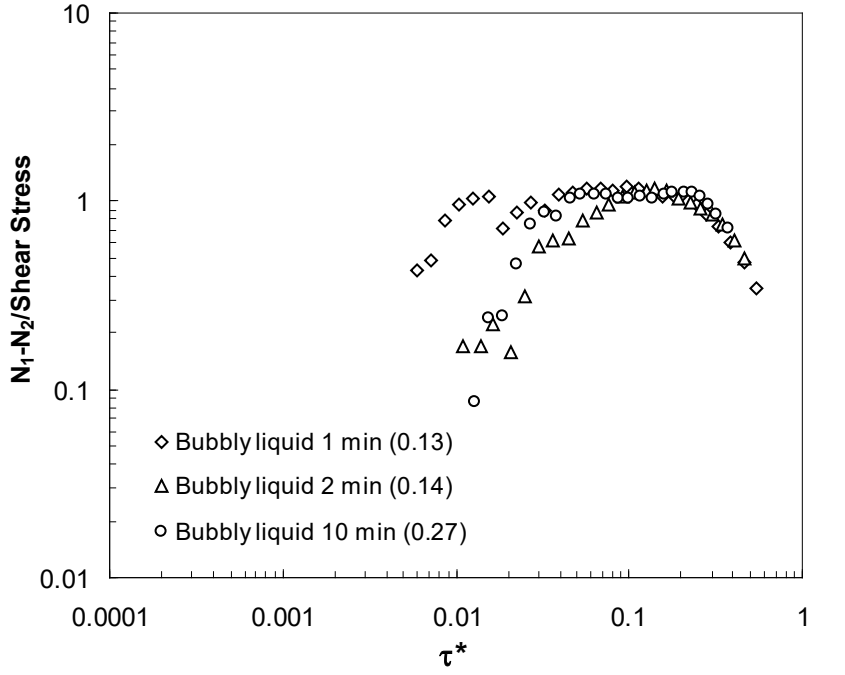

911
912 **Figure 5** Normal and shear stress parameters obtained for honey bubbly liquids for
913 increasing shear rate tests: (*a*) normal stress difference (N_1-N_2), and (*b*) ratio of
914 the measured normal stress difference to shear stress. Solid symbols – honey;
915 open symbols – bubbly liquids. Air volume fraction values are shown in
916 parenthesis for each data set. Dashed locus in (*a*) shows normal stress from
917 inertial effects calculated for honey using Equation [16].
918

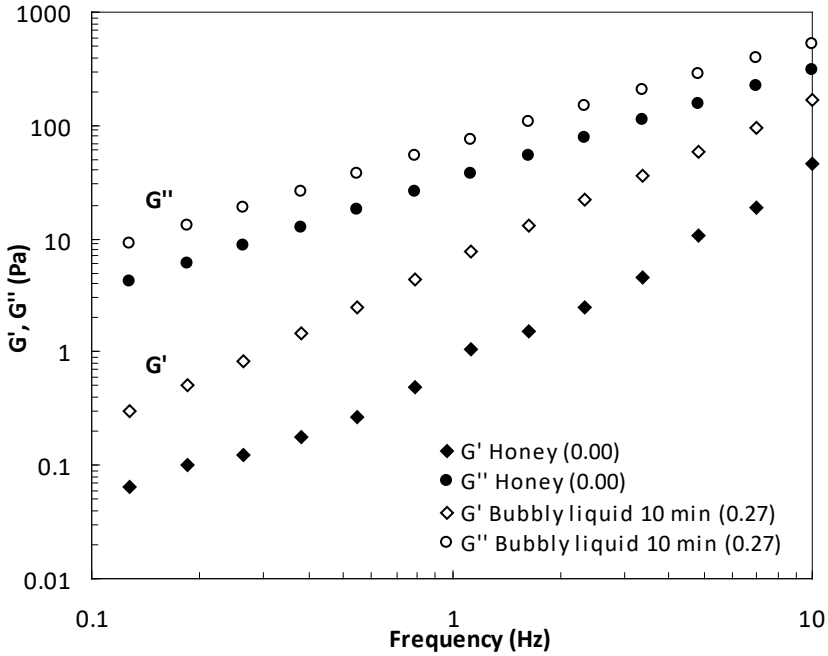

919

920

921 **Figure 6** Dynamic mechanical spectra of honey and bubbly liquids: loss and storage moduli as

922 function of the frequency of oscillation. ϕ values shown in parentheses for each data set.

923

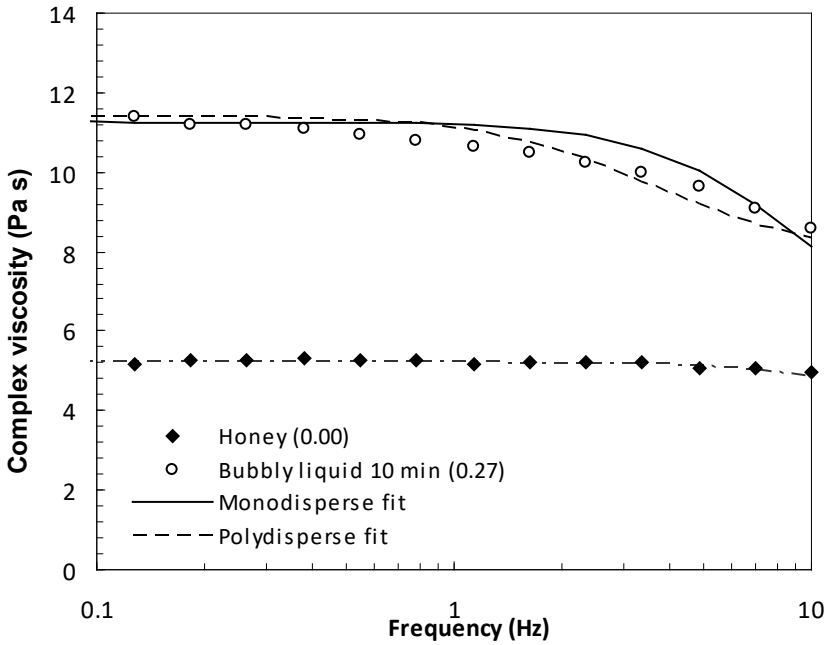

924
925

926 **Figure 7** Comparison of the fit of the monodispersed (solid lines) and polydispersed (dashed lines)
927 forms of the Llewellin *et al*. model to the complex viscosity measured for the honey-based
928 bubbly liquid after 10 min aeration. Solid symbols – honey; open circles – bubbly liquid.
929 Liquid air volume fractions shown in parentheses.

930

(*a*)

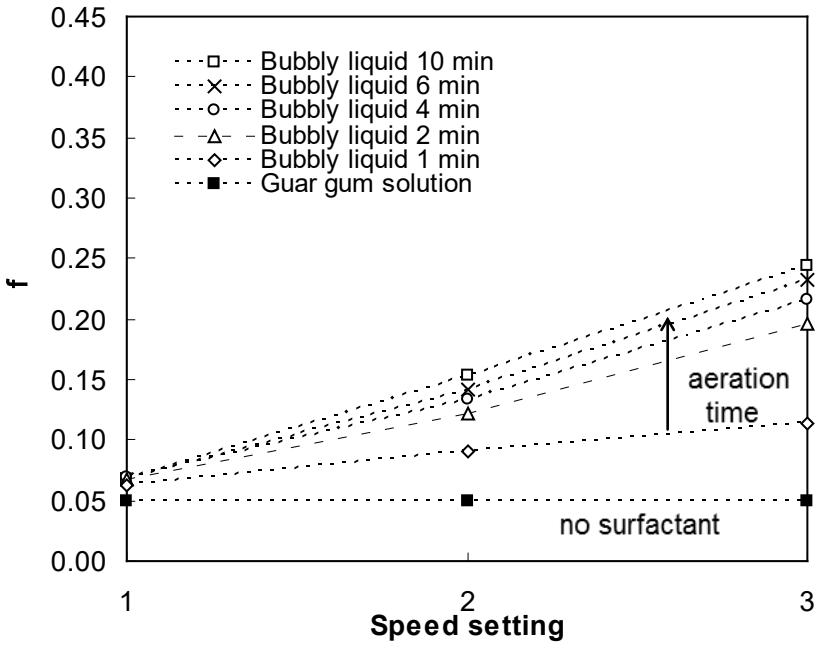

(*b*)

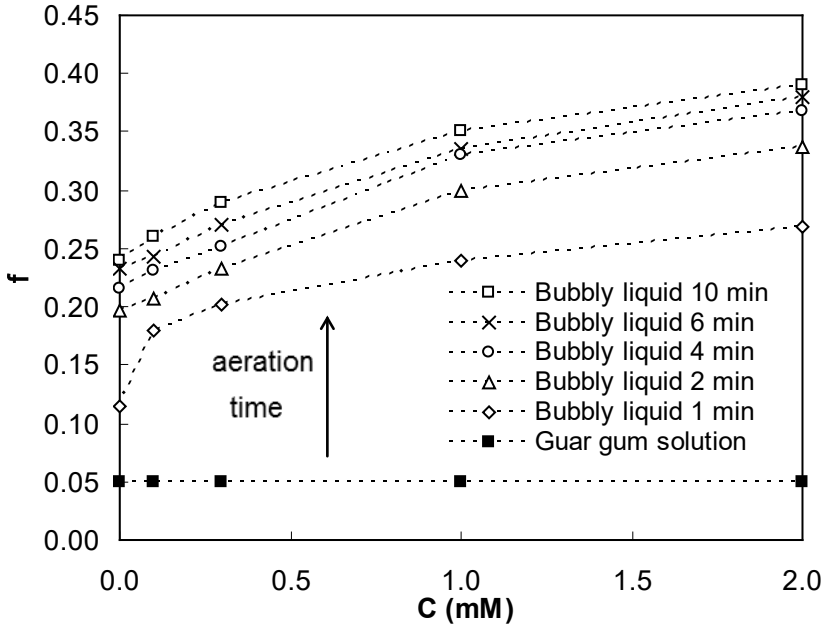

Figure 8 Effect on the air volume fraction of 1 wt% aqueous guar gum solutions of (*a*) mixer speed setting in the absence of surfactant, and (*b*) surfactant concentration at mixer speed 3. Closed symbols – guar gum solution, open – bubbly liquids.

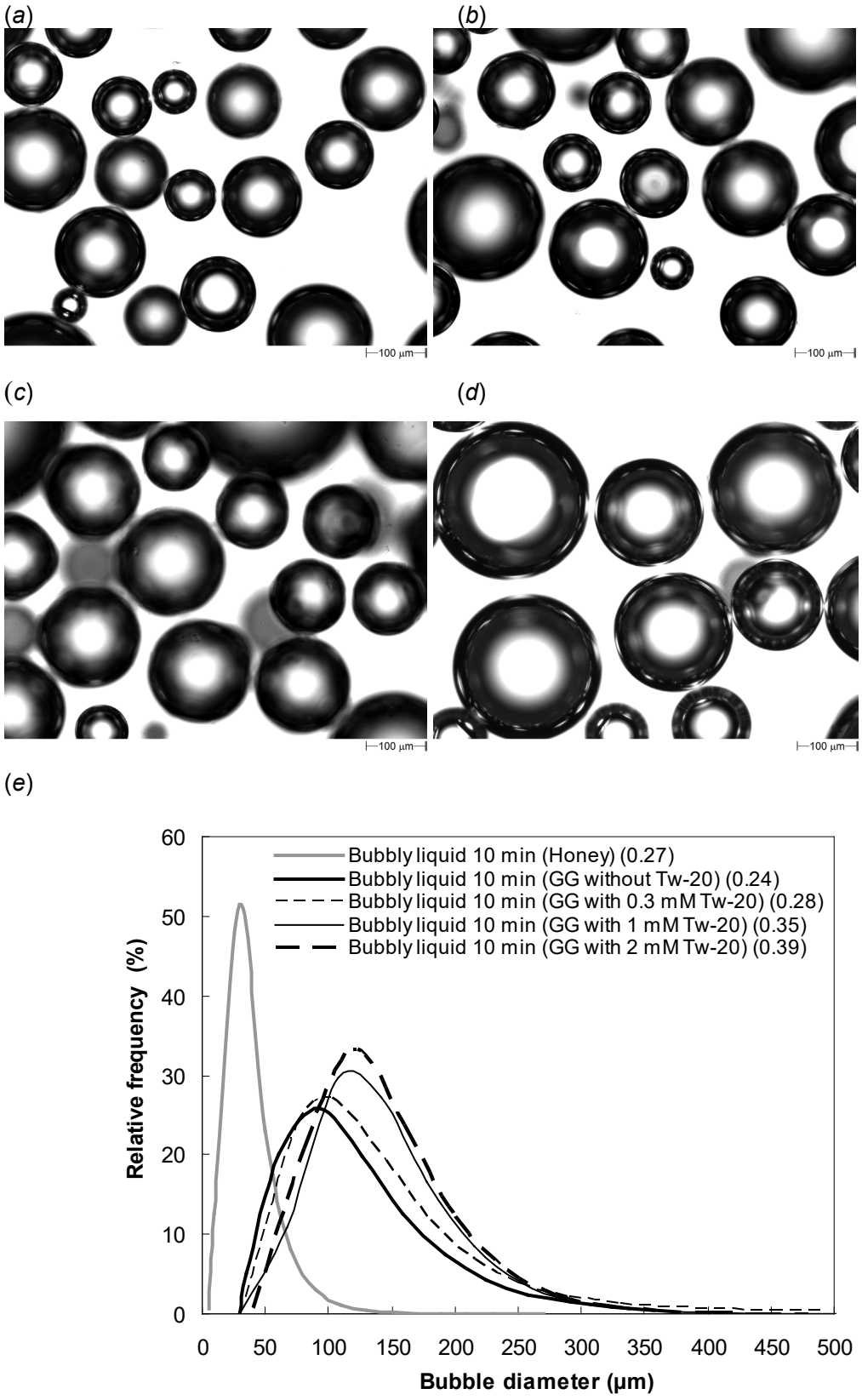

Figure 9 Bubbly liquids prepared with 1.0% w/w guar gum, 10 min aeration: (*a*) without surfactant, and with (*b*) 0.3, (*c*) 1.0, (*d*) 2.0 mM Tween 20. Bubble number size distributions in (*e*) show log-normal fits based on the radii. ϕ values given in parentheses.

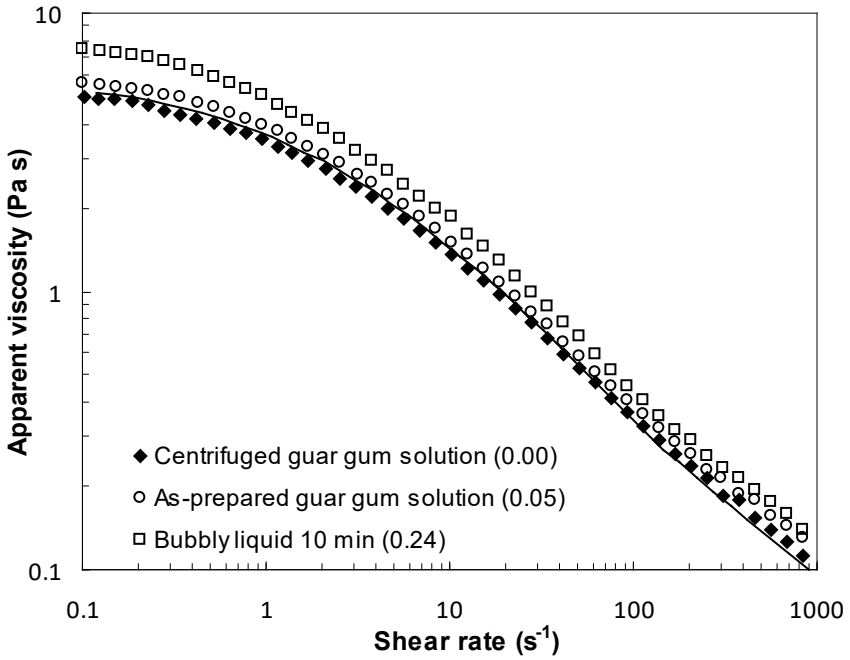

949

950

951 **Figure 10** Flow curves of surfactant-free guar gum solution and bubbly liquids made
952 with guar gum (1.0%, w/w) after different mixing times. Increasing shear rate.
953 Solid symbols - centrifuged solution, open symbols - bubbly liquids (guar gum
954 solution, circles; 10 min aeration, squares). The solid line shows the best fit to
955 the centrifuged solution obtained with the Cross model (Equation [13]). Air
956 volume fraction values are shown in parentheses for each data set.

957

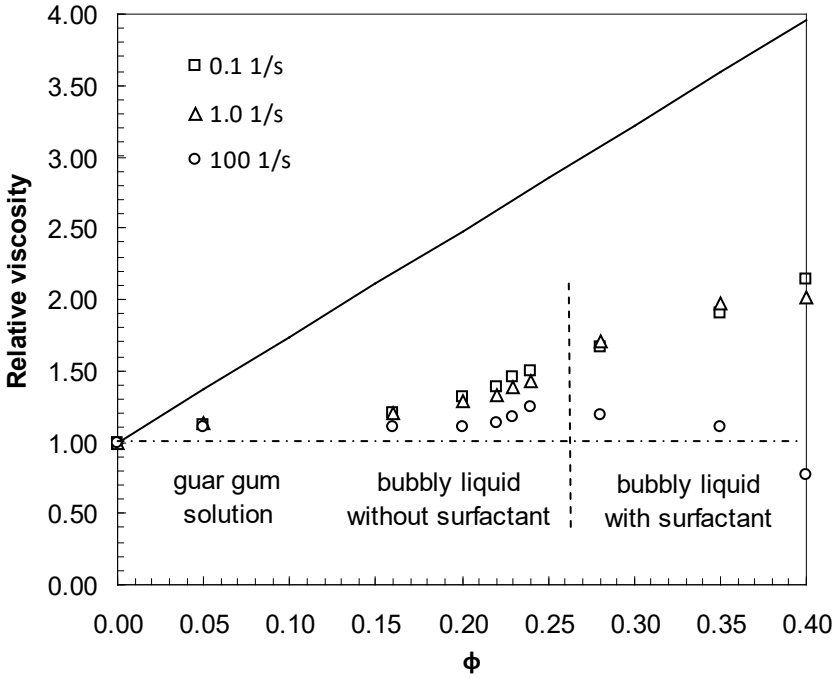

958
959

960 **Figure 11** Effect of air volume fraction on guar gum bubbly liquid relative viscosity at shear rates
961 of 0.1, 1.0 and 100 s^{-1}. Solid line shows linear trend line obtained by regression for honey,
962 with $\eta_r = 1 + 7.4\phi$ ($R^2 = 0.990$).

963

964 (*a*)

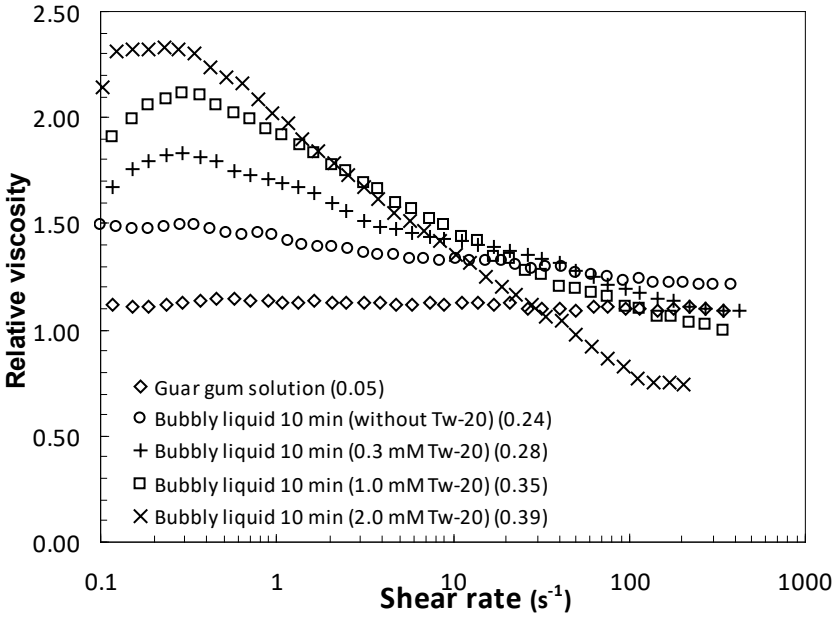

965

966 (*b*)

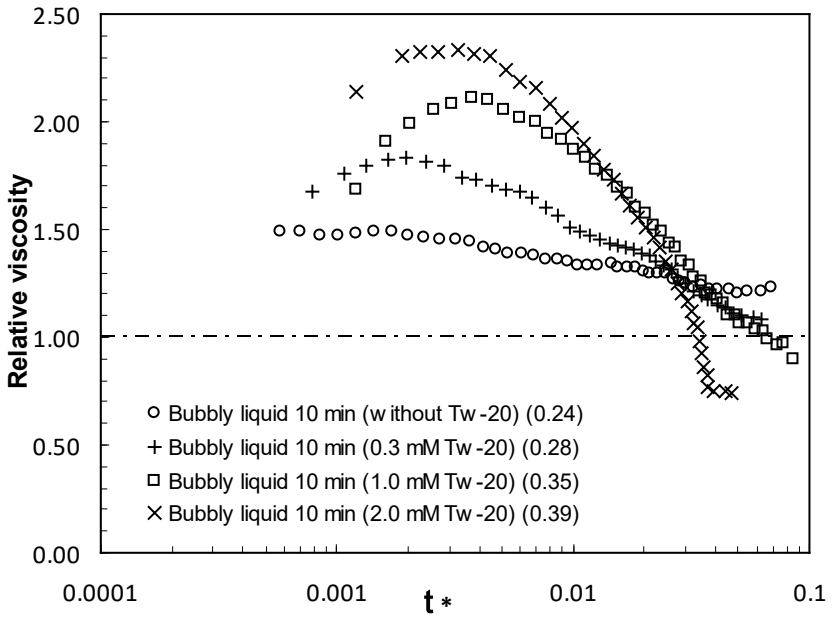

967

968

969 **Figure 12** Relative viscosity of guar gum solutions with surfactant (0.3, 1.0 and 2.0 mM) as a

970 function of (*a*) shear rate and, (*b*) τ^*. Air volume fraction values are shown in parentheses.

971

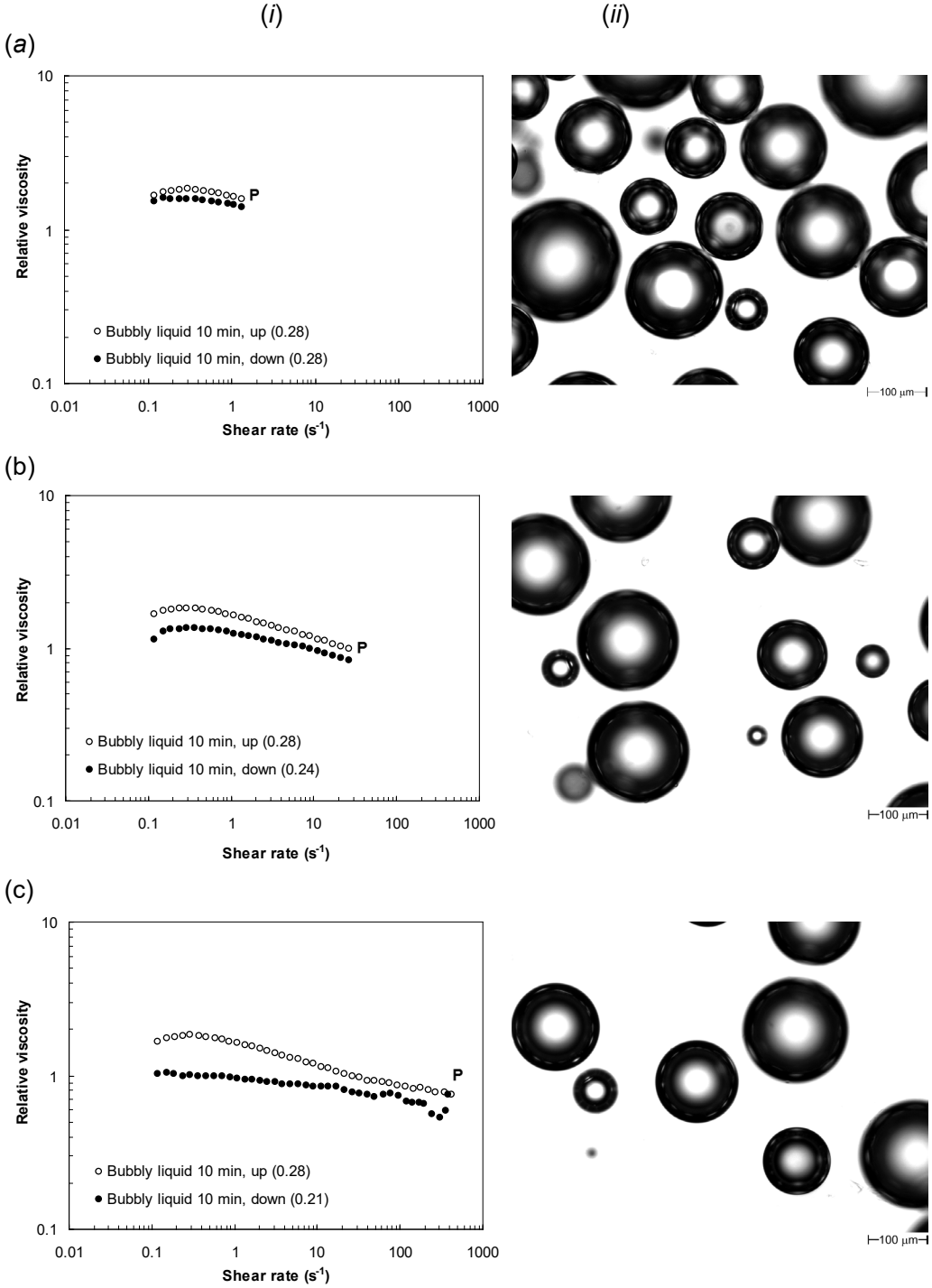

Figure 13 Guar gum bubbly liquids prepared with 0.3 mM surfactant and 10 min aeration: (*i*) flow curves for increasing and then decreasing shear rates; (*ii*) images taken after shearing to a maximum shear rate of (*a*) 1 s^{-1}; (*b*) 30 s^{-1}; (c) 300 s^{-1}. Figure 9(*b*) shows a photograph of the bubbly liquid before testing. Symbols: open circles – measurements at increasing shear rates, closed circles – measurements at decreasing shear rates. Air volume fraction values for each data set are shown in parentheses. Point P – time at which sample was removed and photograph taken.

988 (*a*)

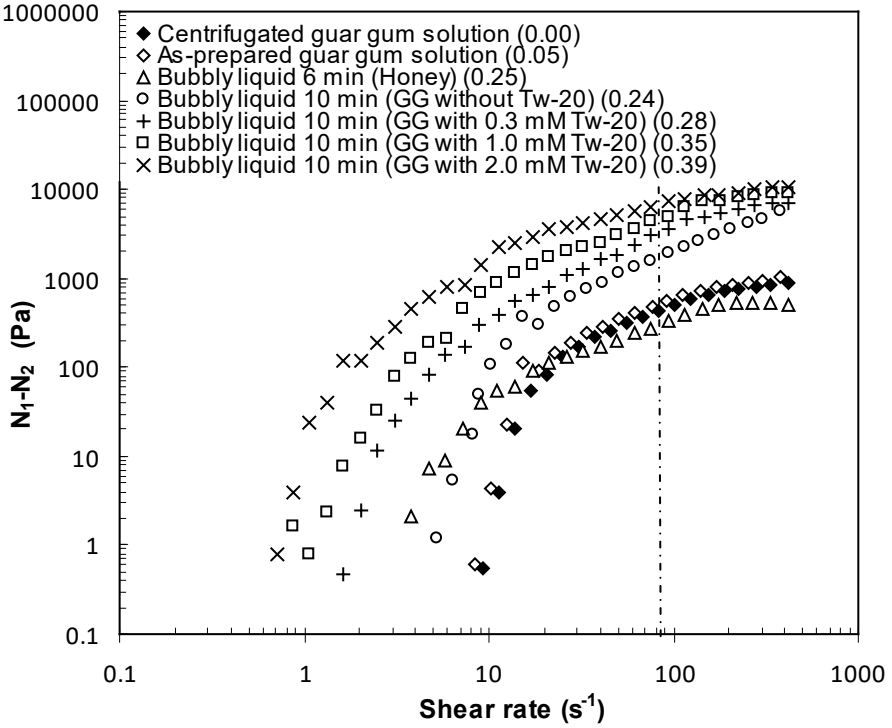

989

990

991 (*b*)

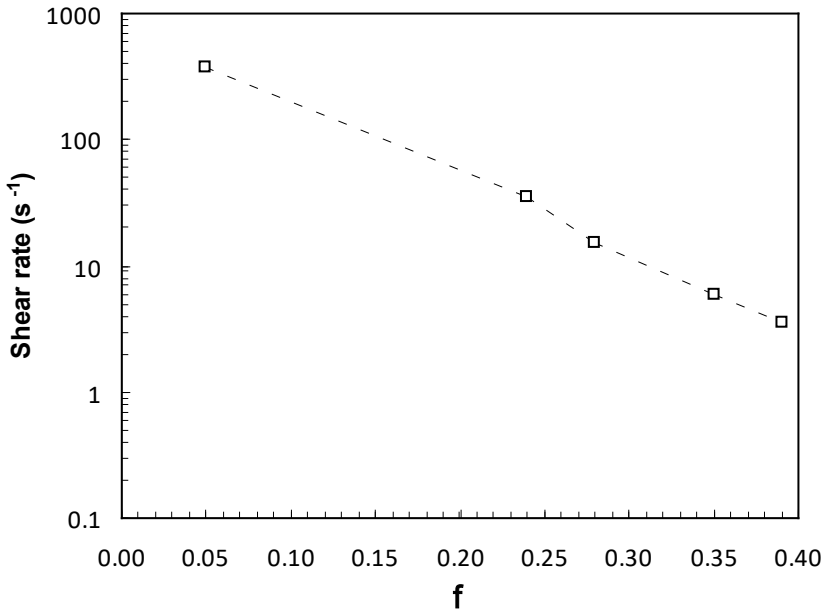

992

993

994

995

(*c*)

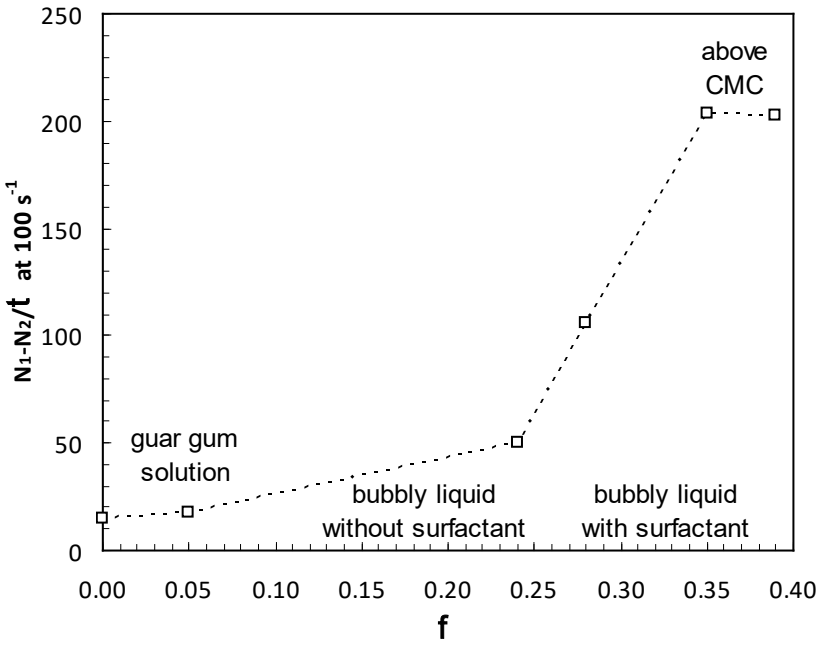

(*d*)

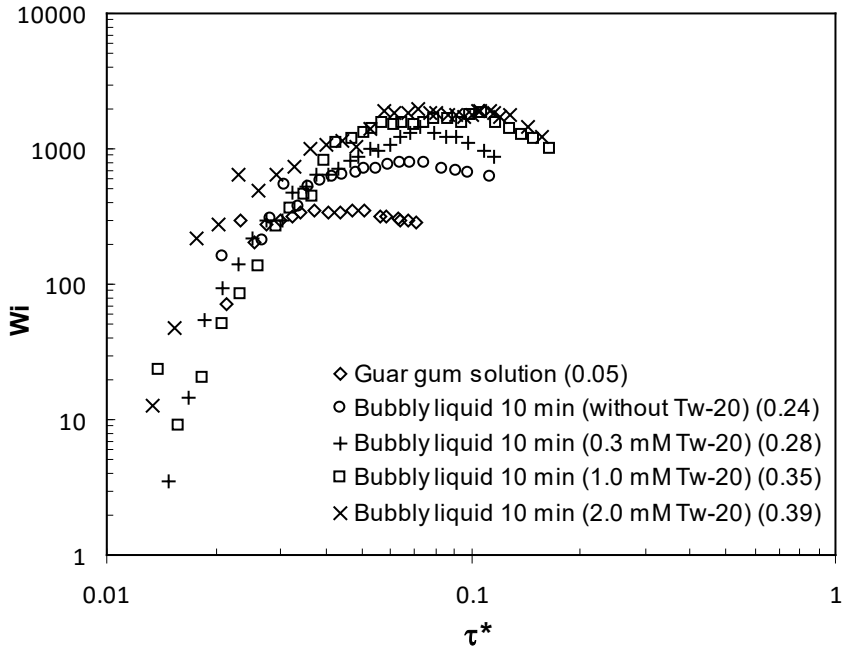

Figure 14 Stress parameters measured for guar gum solutions and bubbly liquids with and without surfactant: (*a*) N_1-N_2, and (*b*) shear rate at which N_1-$N_2 \approx \Gamma/r$; (c) ratio of the measured normal stress difference to shear stress at 100 s^{-1} (marked with a vertical line in (*a*)) at different air volume fractions; (d) estimated Weissenberg number (= (N_1-N_2)/τ) plotted against dimensionless shear stress. ϕ values shown in parentheses for each data set.

(*a*)

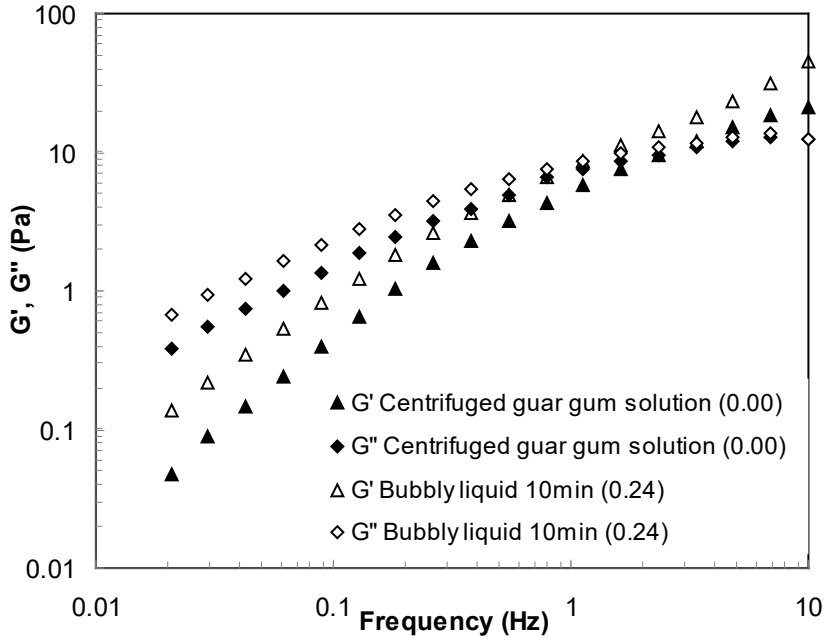

(*b*)

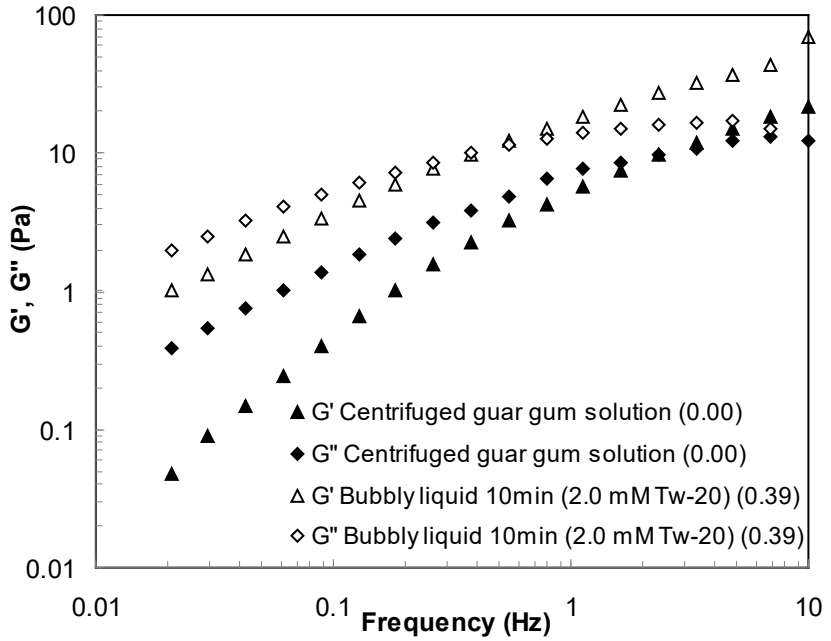

Figure 15 Mechanical spectra of centrifuged 1 wt% guar gum solution and bubbly liquids generated by 10 min aeration (*a*) without and (*b*) with 2.0 mM of surfactant. Symbols: closed – centrifuged guar gum solution, open – bubbly liquids. Air volume fraction values shown in parentheses for each data set.

Table Captions

Table 1 Honey-based bubbly liquids. Air volume fraction, bubble characteristics and fitting parameters

Table 2 Parameter values obtained for Cross-Williamson model, Equation [13], for aqueous guar gum solutions prepared without surfactant

Table 1 Honey-based bubbly liquids. Air volume fraction, bubble characteristics and fitting parameters

					Equation [20] $x = \tau^*$			Equation [6]	Equation [7]
	Aeration time	ϕ	Bubble number, n_b	Mean radius	a_1	a_2	η_{app}†	K	b'
	(min)	(-)		(μm)	(-)	(-)	(Pa s)	(-)	(-)
Honey	-	-	-	-	-	-	5.20±0.01^{c}	-	1.00±0.00^{e}
Bubbly liquid 1 min	1	0.13±0.01^{b}	500±25^{b}	52±3^{b}	1.70±0.05^{b}	2.31±0.01^{d}	6.01±0.09^{b}	35.9±0.1^{d}	1.13±0.01^{d}
Bubbly liquid 2 min	2	0.14±0.01^{b}	550±20^{b}	50±2^{b}	1.91±0.05^{b}	2.62±0.02^{c}	6.22±0.10^{b}	36.8±0.2^{c}	1.17±0.01^{c}
Bubbly liquid 6 min	6	0.25±0.01^{a}	850±40^{a}	42±2^{a}	2.82±0.02^{a}	3.80±0.03^{b}	8.50±0.08^{a}	42.3±0.2^{b}	1.27±0.01^{b}
Bubbly liquid 10 min	10	0.27±0.01^{a}	900±30^{a}	40±3^{a}	2.90±0.04^{a}	4.21±0.02^{a}	8.71±0.07^{a}	45.0±0.3^{a}	1.31±0.01^{a}

♣Data are presented as means ± standard deviation. Data in a column with different superscript letters are significantly different at the $p \leq 0.05$ level

† Apparent viscosity at 1 s^{-1}

Table 2 Parameter values obtained for Cross-Williamson model, Equation [13], for aqueous guar gum solutions prepared without surfactant.[†]

Sample	ϕ (-)	η_0 (Pa s)	k (s^{1-n})	n (-)	R^2	Standard deviation (Pa s)
Centrifuged guar gum solution	0.00±0.00[d]	5.87±0.01[f]	0.61±0.01[c]	0.29±0.00[c]	0.999	0.038
Guar gum solution	0.05±0.00[c]	5.95±0.03[f]	0.61±0.00[c]	0.29±0.01[c]	0.996	0.041
Bubbly liquid 1 min aeration	0.11±0.01[b]	6.23±0.02[e]	0.62±0.01[b,c]	0.28±0.01[c]	0.998	0.039
2 min	0.20±0.00[a]	7.05±0.01[d]	0.65±0.01[b]	0.26±0.01[b,c]	0.997	0.041
4 min	0.22±0.01[a]	7.34±0.03[c]	0.67±0.01[b]	0.25±0.01[a]	0.997	0.042
6 min	0.23±0.01[a]	7.82±0.01[b]	0.69±0.00[b]	0.24±0.01[b,a]	0.994	0.043
10 min	0.24±0.02[a]	8.25±0.05[a]	0.73±0.01[a]	0.22±0.01[a]	0.991	0.047

[†]Data are presented as mean ± standard deviation. Data values in a column with different superscript letters are significantly different at the $p \leq 0.05$ level.